STUDYING APTAMER BINDING TO CANCER CELL MEMBRANE RECEPTORS BY FLUORESCENCE CORRELATION SPECTROSCOPY

By

ALINA C. MUNTEANU

A DISSERTATION PRESENTED TO THE GRADUATE SCHOOL
OF THE UNIVERSITY OF FLORIDA IN PARTIAL FULFILLMENT
OF THE REQUIREMENTS FOR THE DEGREE OF
DOCTOR OF PHILOSOPHY

UNIVERSITY OF FLORIDA

2007

To my Parents

ACKNOWLEDGMENTS

I would like to thank Dr. Weihong Tan for his guidance, support and encouragement during my studies at the University of Florida. Also, I would like to thank the current and former members of the Tan research group for providing invaluable support, encouragement and creating an excellent working environment.

I am extremely thankful to my parents, Maria-Augustina and Ioan Munteanu, for their endless love, support, advice, and encouragement.

The many friends and colleagues I have gained through the years made my life much more pleasant and enjoyable. I would like to thank Tim Drake, for his friendship and support; Chaoyong Yang, for his great personality and willingness to help; Lisa Hilliard, for all her encouragement; Colin Medley, for the helpful discussions; Marie-Carmen Estevez, for becoming such a good friend; and, of course, my adoptive Puerto Rican "family", Karen Martinez, Roberto Reyes, Marie Vicens, and Jose Valle, for their great friendship, support, encouragement, and all the fun times we had outside of the lab.

TABLE OF CONTENTS

page

LIST OF TABLES

Table page

LIST OF FIGURES

Abstract of Dissertation Presented to the Graduate School
of the University of Florida in Partial Fulfillment of the
Requirements for the Degree of Doctor of Philosophy

STUDYING APTAMER BINDING TO CANCER CELL MEMBRANE RECEPTORS BY FLUORESCENCE CORRELATION SPECTROSCOPY

By

Alina C. Munteanu

December 2007

Chair: Weihong Tan
Major: Chemistry

Aptamers are short strands of oligonucleotides, designed to have excellent binding affinity and selectivity towards certain target molecules. Due to their capacity to bind tightly and specifically to their ligands, aptamers have applications in fields ranging from medicine to biochemical research. Fluorescence correlation spectroscopy (FCS) is being recognized as a highly sensitive method for the investigation of molecular interactions. By using this technique, association and dissociation rate constants, and binding constants can be obtained from the analysis of the Brownian motion of fluorescently labeled probes. The present study is focused on cancer cell-specific aptamers binding to their target. For determination of the dissociation rate constant, a binding curve is obtained by incubating the target cells with different concentrations of fluorescently-labeled aptamer. The binding constants are then compared to the ones that have been reported by flow cytometry. Further, a method for calculation of the aptamer receptor density on the cell membrane is proposed. The study will show that FCS is a reliable method for the determination of binding properties of aptamer-target complexes even when used in vivo.

CHAPTER 1
INTRODUCTION

1.1 Aptamers for Cancer Cell Detection

Since the discovery in the early 1980s that RNA was not simply a passive carrier of genetic information but could participate directly in catalysis in living cells,[1,2] our understanding of RNA structure and function has been in constant flux. Another important insight emerged in 1990 when three separate groups used *in vitro* selection approaches to isolate RNA and DNA molecules that bind tightly to several nucleic-acid binding proteins, and to organic dyes used for affinity chromatography.[3–5]

The isolation of novel RNAs that bind to small organic molecules confirmed the assumption — based on the ability of RNA to fold into complex, three-dimensional shapes rivaling those of proteins — that in degenerate sequence libraries of $\geq 10^{15}$ molecules, which are easily created and manipulated in the laboratory, there is probably an RNA molecule which will fold to bind almost any target.[5] A logical extension of this idea was that aptamers that bind transition state analogues that mimic the chemical structure of key intermediates in enzyme catalaysis would also be catalytically active, analogous to catalytic antibodies. This has turned out to be true even for complex organic reactions.[6,7] These results provide compelling experimental evidence in support of the 'RNA world' hypothesis, which postulates that the biological world evolved from a self-replicating RNA molecule that was assembled by chance[8].

An iterative protocol for the *in vitro* selection experiments discussed above[4] was introduced and called 'systematic evolution of ligands by exponential enrichment' (SELEX) (Figure 1-1). The products of the selection[5] were called 'aptamers' (from the Latin *aptus* meaning 'fitting'). By analogy with antibodies the targets bound by aptamers were called 'apatopes', although 'epitope' or 'target' is the most frequently used terminology. The selection

protocol has subsequently been reduced to an automated *in vitro* process,[9–11] opening the way for high-throughput selection against an almost infinite set of targets. The range of aptamer reagents isolated can be assessed by reference to an online database.

Pathologists today diagnose the vast majority of cancers based on the shape or other characteristics of tumor tissue or diseased cells. That is a problem because it often means that cancers may already be advanced when detected.

Normally, definitive diagnosis of cancer requires a visual examination of the tumor, which is an invasive and time-consuming process. Most importantly, this process is not suitable for early detection, when the cancer is at its most treatable.

Clinicians can sometimes use antibodies, proteins that recognize and fight bodily intruders, to identify different types of cancer. That is the case, for example, with the prostate-specific antigen test for prostate cancer. Antibodies are preferable to diagnosis by appearance because they are consistent and accurate, but they are only available for a selected few cancers.

Scientists know that cancer tissue has a unique molecular fingerprint that can distinguish it from healthy tissue. But attempts to target cells via these fingerprints have largely proved futile because there are few molecular tools to recognize the fingerprints. The aptamers exploit the differences on the surface of cells to discern cancerous ones. Key to the approach is it does not require prior knowledge of cancer indicators.

Using the cell-based aptamer selection strategy, aptamers which can specifically recognize any kind of cells without prior knowledge of molecular changes associated with the disease can be generated.[12] In experiments, the researchers showed they could successfully design sets of aptamers that would recognize leukemia cells that had been mixed in with normal bone marrow cells. The aptamers also successfully distinguished leukemia T-cells from lymphoma B-cells.

Both results indicate that the aptamer method could be used to identify many different types of cancer.

1.2 Cell Membrane Binding Studies

Numerous biochemical processes are mediated by interactions between soluble ligands and cell-surface receptors. Considerable effort has been devoted to understanding the role of ligand-receptor interactions in the mechanisms of these processes. A series of theoretical investigations into the thermodynamic, kinetic, and transport characteristics of interactions between macromolecules in three-dimensional solution and sites on a planar or spherical surface has been presented[13-27]. These investigations have suggested that a phenomenon of particular importance is the process in which reversibly bound ligands dissociate from receptors, diffuse for a time in the nearby solution, and then rebind to the same or a nearby receptor on the cell surface. Evidence for the rebinding process has been experimentally obtained for a variety of ligand-receptor systems, including haptens with IgE-coated mast cells[28-30]; bovine prothrombin fragment 1 with negatively charged substrate-supported planar membranes[31]; antibodies with immobilized peptides[32]; lipoprotein lipase with immobilized heparin sulfate[33]; and neurotransmitters in synapses[34].

1.3 Fluorescence

When specimens, living or non-living, organic or inorganic, absorb and subsequently re-radiate light, the process is described as photoluminescence. If the emission of light persists for up to a few seconds after the excitation energy (light) is discontinued, the phenomenon is known as phosphorescence. Fluorescence, on the other hand, describes light emission that continues only during the absorption of the excitation light. The time interval between absorption of excitation light and emission of re-radiated light in fluorescence is of extraordinarily short duration, usually less than a millionth of a second.

The phenomenon of fluorescence was known by the middle of the nineteenth century. British scientist Sir George G. Stokes first made the observation that the mineral fluorspar exhibits fluorescence when illuminated with ultraviolet light, and he coined the word "fluorescence." Stokes observed that the fluorescing light has longer wavelengths than the excitation light, a phenomenon that has become to be known as the Stokes shift.

Fluorescence microscopy is an excellent method of studying material that can be made to fluoresce, either in its natural form (termed primary or autofluorescence) or when treated with chemicals capable of fluorescing (known as secondary fluorescence).

Fluorochromes are stains, which attach themselves to visible or sub-visible organic matter. These fluorochromes, capable of absorbing and then re-radiating light, are often highly specific in their attachment targeting and have significant yield in absorption-emission ratios (a concept termed quantum yield). This makes fluorochromes extremely valuable in biological applications. The growth in the use of fluorescence microscopes is closely linked to the development of hundreds of fluorochromes with known intensity curves of excitation (absorption) and emission and well-understood biological structure targets.

Once a molecule has absorbed energy in the form of electromagnetic radiation, there are a number of routes by which it can return to ground state (Figure 1-2).

1.4 Fluorescence Correlation Spectroscopy (FCS)

Fluorescence correlation spectroscopy (FCS) is an experimental technique, developed to study kinetic processes through the statistical analysis of equilibrium fluctuations. A fluorescence signal is coupled to the different states of the system of interest, so that spontaneous fluctuations in the system's state generate variations in fluorescence. The autocorrelation function of fluctuations in fluorescence emission carries information on the characteristic time scales and the relative weights of different transitions in the system. Thus, with the appropriate

model of the system dynamics, different characteristic kinetic rates can be measured. For example, fluctuations in the number of fluorescent particles unravel the diffusion dynamics in the sampling volume.

Since its invention in 1972,[35] FCS has known the classical age: chemical rates of binding–unbinding reactions as well as coefficients of translational and rotational diffusion have been measured.[36]

However, although the principal ideas behind FCS as well as its main applications were already established at that stage, the technique was still rather cumbersome and poorly sensitive, requiring high concentrations of fluorescent molecules. Its renaissance came in 1993 with the introduction of the confocal illumination scheme in FCS.[37] This work generated a great many technical improvements, pushed the sensitivity of the technique to the single-molecule level and led to a renewed interest in FCS. The efficient detection of emitted photons extended the range of applications and allowed one to probe the conformational fluctuations of biomolecules and the photodynamical properties of fluorescent dyes. Finally, FCS recently entered the industrial age with the introduction of Zeiss and Evotech's Confocor commercial instrument, and its common use in drug-screening assays.

A number of recent short reviews[38-42] on the different aspects of FCS attests to the popularity of the technique.

1.4.1 Molecular Studies

FCS is a technique which relies on the fact that thermal noise, usually a source of annoyance in an experimental measurement, can be used to the profit of an experimentalist to glean some information on the system under study.

The understanding of the fluctuation–relaxation relationship in thermodynamics has been a great achievement of statistical physics. The theory of Brownian movement not only established

a macroscopic understanding of the consequences of the existence of the atom, but also opened up a whole new area of research related to the study of systems near equilibrium. The experimental support for this atomistic theory came with Perrin's observation of Brownian particles of mastic under a microscope.[43] Macroscopic dynamical properties (the viscosity of the fluid) were derived from microscopic fluctuations (the diffusion of the probe).

The explicit formulation of the fluctuation–dissipation theorem states that the dynamics governing the relaxation of a system out of equilibrium are embedded in the equilibrium statistics. In the spirit of this theory, Eigen and followers developed the temperature-jump technique, where the relaxation of a system after thermal perturbation gives insight into the thermodynamic equilibrium. Classically, the temperature jump is generated by capacitance discharge or laser-pulse absorption, and the relaxation towards equilibrium is monitored by spectroscopy (e.g. UV absorption or circular dichroism).

Another perturbative technique has been introduced to measure the diffusion of biomolecules. Fluorescence recovery after photobleaching (FRAP), as its name implies, consists in monitoring the dynamics of fluorescence restoration after photolysis, due to the diffusion influx from neighbouring areas. This photodestructive method has been very successful in application to living cells, specifically to analyze the dynamics of membrane trafficking.

Less invasive techniques, such as quasi-elastic light scattering (QELS), are also used to get dynamic information from monitoring the fluctuations of the refraction index.[44] However, QELS is poorly sensitive to changes on the molecular level, while the other techniques discussed (temperature jump and FRAP) are perturbative.

A widely used method to study changes on a molecular scale (10–100 Å) is based on the fluorescence resonance energy transfer (FRET): a transfer of an excitation between two different

fluorophores (donor and acceptor), whose corresponding emission (donor) and excitation (acceptor) spectra overlap. The efficiency of energy transfer depends strongly on the distance between the donor and the acceptor: hence one can take advantage of FRET to follow the association of two interacting molecules or to monitor the distance between two sites within a macromolecule when labeled with two appropriate dyes.[45]

FCS corrects the shortcomings of its precursors, as it monitors the relaxation of fluctuations around the equilibrium state in a non-invasive fashion. It relies on the robust and specific signal provided by fluorescent particles to analyze their motions and interactions. In combination with FRET, FCS further allows one to probe the dynamics of intra-molecular motions.

1.4.2 The First Implementation of FCS

Magde *et al*[35] invented FCS in 1972 and showed its feasibility by monitoring the fluctuations in the chemical equilibrium of the binding reaction of ethidium bromide to doublestranded DNA. Ethidium bromide (EtBr) is a small intercalating dye, whose fluorescence quantum yield increases by a factor of 20 upon insertion between DNA bases. Thus they studied the binding equilibrium by monitoring the fluorescence fluctuations of the dye.

The original implementation of FCS used laser excitation of 6 kW cm^{-2} at 514.5 nm.

Fluorescence was collected by a parabolic reflector, filtered from the scattered excitation light with a $K_2Cr_2O_7$ solution, and detected with a photomultiplier tube. The analogue fluorescence signal was then analysed with two 100-channel correlators. The typical concentrations were 5 μmol for the ethidium bromide, and 5 nmol for the sonicated calf-thymus DNA of 20 kDa.

The dimensions of the collection volume were 5 μm transversally and 150 μm longitudinally, thus there were about 104 molecules in the field of view. The resulting time

scales of relaxation for the autocorrelation function of the collected fluorescence were in the 10–100 ms range.

There were two sources of fluorescence fluctuations in this experiment: diffusion of the molecules in/out of the sampling volume, and chemical fluctuations associated with the binding/unbinding of EtBr. Correspondingly, the FCS autocorrelation function is a convolution of diffusion and chemical relaxation terms.

The relaxation rate R, characteristic of the binding/unbinding, was deduced from the fits to the fluorescence autocorrelation function and was linearly dependent on the EtBr concentration. This dependence was measured to yield k_{binding}.

This benchmark experiment proved the feasibility of assessing parameters of chemical kinetics through the analysis of equilibrium fluctuations and it set the groundwork for the following implementations of FCS and other related techniques.

In the following sections, the general formalism of FCS measurement will be introduced (Chapter 2). Then the home-built experimental setup for FCS will be described, with practical considerations on its implementation (Chapter 3). The FCS study of the kinetics of aptamer-cancer cell binding will be presented in Chapter 4 and Chapter 5, respectively.

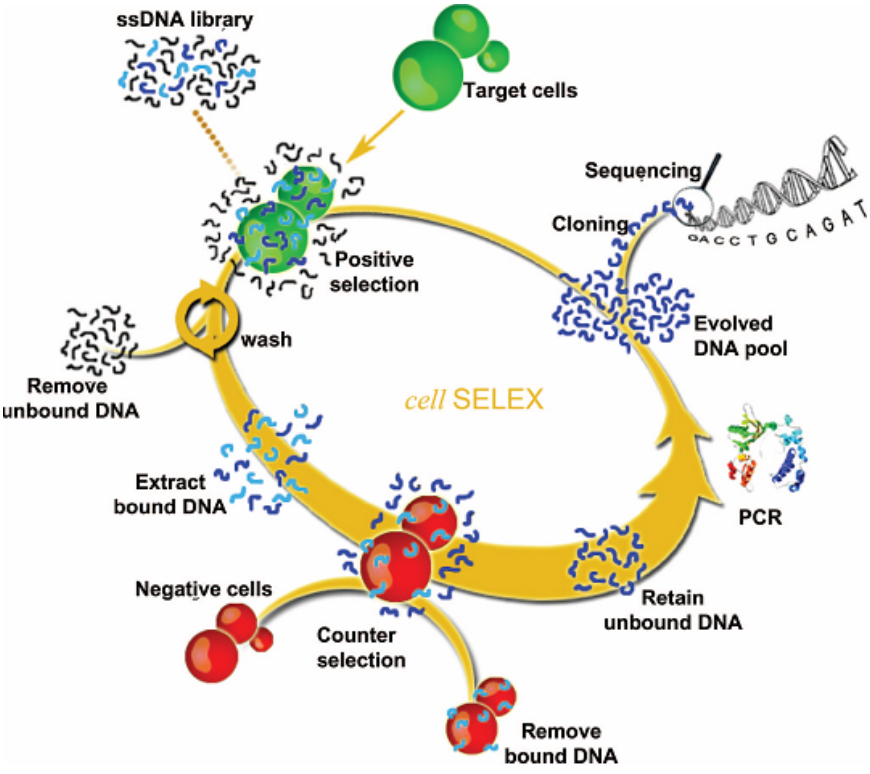

Figure 1-1. Basic outline of a single SELEX cycle. A nucleic-acid library is incubated with the target cells. Target-bound nucleic acids are partitioned and species with lower binding affinity are removed. The bound species are then incubated with non-target cells, and this time the bound nucleic acids are removed. The unbound species are eluted, allowing preferential amplification of higher affinity species. This enriched pool is then used as the starting point in subsequent cycles.

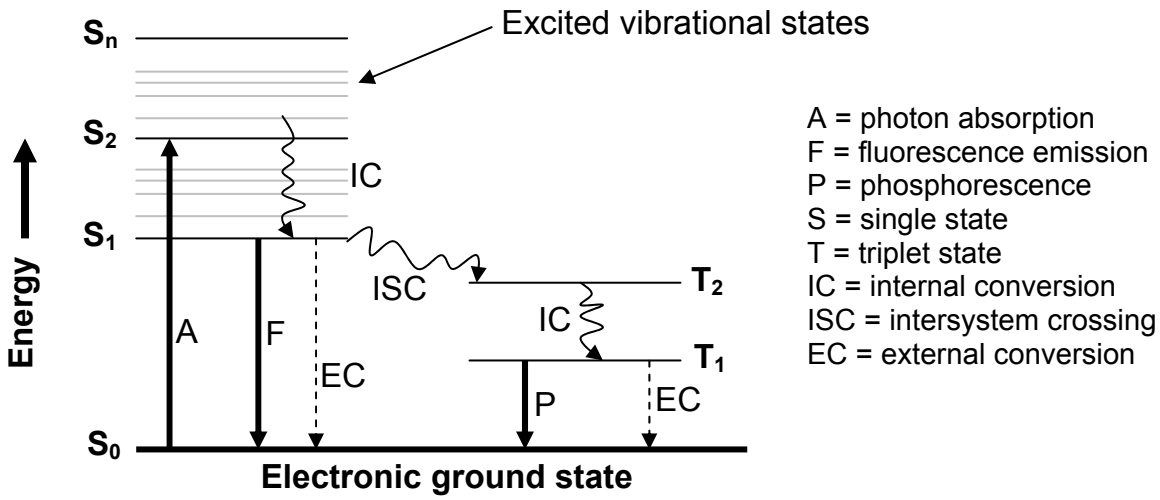

Figure 1-2. Jablonski diagram

CHAPTER 2
THEORY OF FLUORESCENCE CORRELATION SPECTROSCOPY

Fluorescence correlation spectroscopy (FCS) is a technique based on statistical analysis of equilibrium fluctuations. As illustrated in Figure 2-1, at equilibrium, fluorescent molecules move through an illuminated volume element and/or undergo transitions between different states, leading to temporal fluctuations in the fluorescence signal measured from the region. The temporal autocorrelation of the fluorescence fluctuations decays with time. The rate and shape of the decay of the autocorrelation function give information about the time scales and mechanisms of the processes generating the fluorescence fluctuations. Thus, with an appropriate model of the system dynamics, characteristic kinetic rates of different events can be measured.

2.1 History of FCS

FCS relies on the fact that thermal noise can be used as a source of information on the system under study.

Thus, the first great discovery that helped in developing the technique was the Brownian motion of molecules: microscopic particles suspended in liquids move around due to collisions with the surrounding solvent molecules. In his papers treating the theory of Brownian movement, Albert Einstein showed that Brownian diffusion can be explained by the random thermal motion of the water molecules. One of Einstein's most important predictions was that, on average, the displacement of a particle should be proportional to the square root of the diffusion time. This prediction was later experimentally verified by Jean Perrin, who carried out a series of optical microscopy experiments to directly observe the displacements of microscopic particles in water. Einstein's and Perrin's studies provided the most compelling evidence then to be had

about the reality of atoms and molecules. It was also the first time that a fluctuating signal was analyzed to study the molecular scale properties of a system, and hence can be seen as the very first "molecular fluctuation analysis".

In the late 1960's and early 1970's, soon after the invention of the laser, a major advance in the ability to measure the diffusion characteristics of microscopic and sub-microscopic particles occurred with the development of dynamic light scattering (DLS).

Beginning in 1972, Elson, Magde, and Webb[35] published a series of papers describing a fluorescence-based analogue of DLS, which they referred to as fluorescence correlation spectroscopy. The authors realized that using fluorescence measurements to analyze the particle motion has several key advantages over conventional DLS. Fluorescence is more chemically selective than light scattering and allows greater flexibility in studying the motion of specific analytes. Also, fluorescence can be detected from molecules that are much too small to be detected by DLS, which allows one to characterize the motion of small molecules as well as large macromolecules. Finally, fluorescence analysis allows characterizing chemically reacting systems. Chemical reactions generally do not create a large enough index of refraction change to be studied by DLS. However, spontaneous chemical reactions can create fluctuations in the molecular diffusion properties and/or other fluorescence characteristics that could be analyzed via fluorescence detection with much greater sensitivity.

In spite of its successful demonstration, and all of its potential advantages, FCS was not practical to implement in those early years. DLS had the advantage of being able to analyze the motion of many uncorrelated particles at once through the interference of multiple scattered light waves. Since fluorescence emission is incoherent, fluorescence

from multiple fluorophores does not produce such effects. The only effective way to analyze molecular motion by fluorescence is to monitor the individual molecules themselves, and this was not possible in the 1970s. A major problem was that the detection volume was much too large. One of the main sources of background noise in single molecule fluorescence spectroscopy is scattering of the excitation laser by the solvent. Since the backscattered light intensity is proportional to the size of the detection volume, the smaller the detection volume the better. In the early days of FCS, detection volumes of picoliters or greater were employed, whereas modern FCS instruments utilize femtoliter-sized detection volumes. Thus, the backscattered light intensity exceeded the fluorescence emission of an individual molecule. Another problem was that the light collection and detection efficiencies were too poor to detect the fluorescence emitted by a single fluorophor. In order to detect any signal, it was necessary to probe ~10^3 to 10^4 fluorophors at a time, resulting in a large average fluorescence signal. Long data acquisition times, on the order of tens of minutes to hours, were needed in order to average out the signal from interfering noise sources and allow the small variations in the average fluorescence signal to be observed. Thus, given its practical limitations, the technique did not come into widespread use for a number of years.

The crucial advance that revitalized FCS was its combination with single molecule confocal microscopy. Rigler and co-workers were the first to recognize that confocal microscopy, when used as a spectroscopic analysis tool, had great potential for overcoming many of the challenges originally encountered with the earlier versions of FCS. The earliest papers on this subject date back to 1992. Beginning in 1994, Rigler and co-workers[38] and Zare and co-workers[39] demonstrated that confocal microscopy could be

used to directly detect the fluorescence emitted by individual molecules as they diffused through the microscopic focal volume of the confocal microscope. This was an important extension of the original single molecule detection studies reported by Keller and co-workers. With this discovery, the correlation function could be determined based on a relatively small number of single molecule fluorescence signals, detected over a period of a few seconds. The dramatic rise in the publication rate of FCS related papers that occurred after these dates attests to the impact of these important discoveries.

A number of books and review articles on single molecule fluorescence detection in solution and its application to FCS have been published over the years that detail these advances.

2.2 Theory of FCS

In this section, the autocorrelation function will be directly computed by taking into account the physical and chemical fluctuations.[40] The kinetic coefficients considered are diffusion coefficient and chemical rates which will in turn determine the shape of the autocorrelation function.

2.2.1 General Formalism

We consider an ideal solution of *m* chemical components. Component *j* is characterized by its local concentration $C_j(\vec{r}, t)$, its ensemble average concentration $\overline{C}_j = \langle C_j(\vec{r}, t) \rangle$ and the local deviation $\delta C_j(\vec{r}, t) = C_j(\vec{r}, t) - \overline{C}_j$.

Near equilibrium, the equation for the relaxation of δC_j can be written as

$$\frac{\partial \delta C_j(\vec{r}, t)}{\partial t} = D_j \nabla^2 \delta C_j(\vec{r}, t) + \sum_{k=1}^{m} K_{jk} \delta C_k(\vec{r}, t) \qquad (2\text{-}1)$$

where the first term accounts for diffusion and the second term describes the chemical changes, and where the coefficients K_{jk} are combined from the chemical rate constants and the equilibrium concentrations of the species.

The distribution of the excitation light in the sample is denoted by $I(\vec{r})$ (in fact, $I(\vec{r})$ is determined by both the illumination and the detection optical paths). We assume that the number of photons emitted and collected from each of the molecules is proportional to $I(\vec{r})$, so that the number of collected photons per acquisition time per sample Δt is

$$n(t) = \Delta t \int \mathrm{d}^3\vec{r}\, I(\vec{r}) \sum_{k=1}^{m} Q_k C_k(\vec{r}, t) \tag{2-2}$$

where Q_k is the product of the absorption cross section by the fluorescence quantum yield and the efficiency of fluorescence for the component k. Here, we do not consider shot noise as it is uncorrelated and does not contribute to $G(t)$. The deviation $\delta n(t)$ of the photon count from the mean $\bar{n} = \langle n(t) \rangle$ is

$$\delta n(t) = n(t) - \bar{n} = \Delta t \int \mathrm{d}^3\vec{r}\, I(\vec{r}) \sum_{k=1}^{m} Q_k \delta C_k(\vec{r}, t) \tag{2-3}$$

In FCS experiments, $G(t)$ is determined as a time average of the products of the intensity fluctuations and normalized by the square of the average intensity:

$$G(t) = \frac{1}{\bar{n}^2 T} \sum_{i=0}^{T-1} \delta n(t') \delta n(t' + t) \tag{2-4}$$

where T is the total number of accumulated sampling intervals Δt ($T\,\Delta t$ is the total duration of the experiment), t corresponds to delay channel m of the correlator such that $m = t/\Delta t$; $\delta n(t') = n_i - \bar{n}$, $\delta n(t' + t) = n_{i+m} - \bar{n}$, where n_i, n_{i+m} are the numbers of photon counts sampled at times $t' = i\,\Delta t$ and $t' + t = (i + m)\,\Delta t$, respectively.

For the purpose of derivation we will use the ergodicity of the system to write (2-4) as an ensemble average:

$$G(t) = \frac{1}{\bar{n}^2}\langle \delta n(0)\, \delta n(t)\rangle \tag{2-5}$$

Substituting (2-3) into (2-5) we obtain

$$G(t) = \frac{(\Delta t)^2}{\bar{n}^2}\iint \mathrm{d}^3\vec{r}\,\mathrm{d}^3\vec{r}'\, I(\vec{r})I(\vec{r}')\sum_{j,l} Q_j Q_l \langle \delta C_j(\vec{r},0)\delta C_l(\vec{r}',t)\rangle \tag{2-6}$$

Thus the autocorrelation function of intensity fluctuations is a convolution of the auto- and cross-correlation functions of the concentration fluctuations with the excitation profile.

In the following we will use the fact that $\delta C_l(\vec{r}, t)$ are the solutions of equation (2-1) with the initial condition $\delta C_l(r, 0)$ in order to express $\langle \delta C_j(r, 0)\, \delta C_l(r', t)\rangle$ through the combinations of zero-time correlations $\langle \delta C_j(r, 0)\, \delta C_k(r'', 0)\rangle$. The latter can be evaluated from the condition of ideality of the chemical solution: the correlation length being much smaller than the distances between molecules, the positions of different molecules of the same species as well as those of different species are not correlated:

$$\langle \delta C_j(\vec{r},0)\delta C_k(\vec{r}'',0)\rangle = \bar{C}_j \delta_{jk}\delta(\vec{r}-\vec{r}'') \tag{2-7}$$

$\bar{C}_j$ stands here for the mean-square fluctuations of the number $C_j(\vec{r}, t)$ of molecules in a unit volume being equal to its average $\langle C_j(\vec{r}, t)\rangle$ for Poisson statistics.

In order to obtain the solutions $\delta C_j(\vec{r}, t)$ as a function of the initial conditions $\delta C_j(\vec{r}, 0)$, a Fourier transform is applied to equation (2-1):

$$\frac{\mathrm{d}\tilde{C}_l(\vec{q},t)}{\mathrm{d}t} = \sum_{k=1}^{m} M_{lk}\tilde{C}_k(\vec{q},t) \tag{2-8}$$

where

$$\tilde{C}_l(\vec{q},t) = (2\pi)^{-3/2}\int \mathrm{d}^3\vec{r}\,\mathrm{e}^{\mathrm{i}\vec{q}\vec{r}}\delta C_l(\vec{r},t)$$

is a Fourier transform of $\delta C_l(\vec{r}, t)$, and $M_{lk} = T_{lk} - D_l q^2 \delta_{lk}$. The solutions of (2-8) can be represented in a standard way through the eigenvalues $\lambda^{(s)}$ and the corresponding eigenvectors $X^{(s)}$ of the matrix M:

$$\tilde{C}_l(\vec{q},t) = \sum_{s=1}^{m} X_l^{(s)} h_s \exp(\lambda^{(s)} t) \tag{2-9}$$

The coefficients h_s are to be found from the initial conditions:

$$\tilde{C}_l(\vec{q},0) = \sum_{s=1}^{m} X_l^{(s)} h_s$$

Hence,

$$h_s = \sum_{k=1}^{m} (X^{-1})_k^{(s)} \tilde{C}_k(\vec{q},0)$$

and

$$\tilde{C}_l(\vec{q},t) = \sum_{s=1}^{m} X_l^{(s)} \exp(\lambda^{(s)} t) \sum_{k=1}^{m} (X^{-1})_k^{(s)} \tilde{C}_k(\vec{q},0) \tag{2-10}$$

where X^{-1} is the inverse matrix of eigenvectors. Taking into account the fact that the Fourier transform and the ensemble averaging are independent linear operations and thus can be applied in any order, and making use of (2-10) and (2-7), we can evaluate

$$\langle \delta C_j(\vec{r},0)\delta C_l(\vec{r}',t)\rangle = (2\pi)^{-3/2}\int \mathrm{d}^3\vec{q}\,\mathrm{e}^{-\mathrm{i}\vec{q}\vec{r}'}\langle \delta C_j(\vec{r},0)\,\delta C_l(\vec{q},t)\rangle$$

$$= (2\pi)^{-3/2}\int \mathrm{d}^3\vec{q}\,\mathrm{e}^{-\mathrm{i}\vec{q}\vec{r}'}\sum_{s=1}^{m} X_l^{(s)} \exp(\lambda^{(s)} t)\sum_{k=1}^{m} (X^{-1})_k^{(s)} \langle \delta C_j(\vec{r},0)\,\tilde{C}_k(\vec{q},0)\rangle$$

$$= (2\pi)^{-3}\int \mathrm{d}^3\vec{q}\,\mathrm{e}^{-\mathrm{i}\vec{q}\vec{r}'}\sum_{s=1}^{m} X_l^{(s)} \exp(\lambda^{(s)} t)\sum_{k=1}^{m} (X^{-1})_k^{(s)}$$

$$\times \int \mathrm{d}^3\vec{r}''\,\mathrm{e}^{\mathrm{i}\vec{q}\vec{r}''}\langle \delta C_j(\vec{r},0)\delta\tilde{C}_k(\vec{r}'',0)\rangle$$

$$= (2\pi)^{-3}\,\bar{C}_j \int \mathrm{d}^3\vec{q}\,\mathrm{e}^{\mathrm{i}\vec{q}(\vec{r}-\vec{r}')} \sum_{s=1}^{m} X_l^{(s)} \exp(\lambda^{(s)} t)(X^{-1})_j^{(s)} \qquad (2\text{-}11)$$

Finally, substituting (2-11) into (2-6) and carrying out the integration over $\vec{r}$ and $\vec{r}'$, we obtain

$$G(t) = \frac{(\Delta t)^2}{\bar{n}^2} \int \mathrm{d}^3\vec{q}\,|\tilde{I}(\vec{q})|^2 \sum_{j,l} Q_j Q_l \bar{C}_j \sum_s X_l^{(s)} \exp(\lambda^{(s)} t)(X^{-1})_j^{(s)} \qquad (2\text{-}12)$$

where

$$\tilde{I}(\vec{q}) = (2\pi)^{-3/2} \int \mathrm{d}^3\vec{r}\,\mathrm{e}^{-\mathrm{i}\vec{q}\vec{r}}\, I(\vec{r})$$

is the Fourier transform of $I(\vec{r})$. The average number $\bar{n}$ of the collected photons in (2-12) is determined from (2-2):

$$\bar{n} = \Delta t \int \mathrm{d}^3 r\, I(\vec{r}) \sum_{i=1}^{m} q_i \bar{C}_i = (2\pi)^{3/2}\, \tilde{I}(0)\, \Delta t \sum_{i=1}^{m} q_i \bar{C}_i \qquad (2\text{-}13)$$

Thus *G(t)* can be evaluated from the parameters of the experimental setup and from diffusion coefficients, chemical rates and concentrations of the chemical components of a sample.

In many realizations of FCS, a confocal illumination/detection optical setup is used such that *G(t)* can be calculated explicitly by assuming a Gaussian illumination intensity profile:

$$I(\vec{r}) = I_0 \exp\left(-\frac{2\left(x^2 + y^2\right)}{w_{xy}^2} - \frac{2z^2}{w_z^2}\right) \qquad (2\text{-}14)$$

where w_z and w_{xy} are the sizes of the beam waist in the direction of the propagation of light and in the perpendicular direction, respectively (normally $w_z > w_{xy}$).

Then, the Fourier transform of the illumination/collection profile is

$$\tilde{I}(\vec{q}) = \frac{I_0 w_{xy}^2 w_z}{8} \exp\left(-\frac{w_{xy}^2}{8}\left(q_x^2 + q_y^2\right) - \frac{w_z^2}{8} q_z^2\right) \tag{2-15}$$

and from (2-12), (2-13) and (2-15):

$$G(t) = \frac{(2\pi)^{-3}}{\left(\sum Q_i \bar{C}_i\right)^2} \int \mathrm{d}^3\vec{q} \, \exp\left(-\frac{w_{xy}^2}{4}\left(q_x^2 + q_y^2\right) - \frac{w_z^2}{4} q_z^2\right)$$

$$\times \sum_{j,l} Q_j Q_l \bar{C}_j \sum_s X_l^{(s)} \exp(\lambda^{(s)} t)(X^{-1})_j^{(s)} \tag{2-16}$$

For each particular case *G(t)* can be computed from the general expression (2-16) by evaluating the $\vec{q}$ dependence of the eigenvalues for the relaxation dynamics.

2.2.2 Single-Component Diffusion

In the case of diffusion of a single chemical species in a dilute solution, the system of equation (2-1) consists of a single diffusion equation (all of the subscripts will be omitted):

$$\frac{\partial \delta C(\vec{r}, t)}{\partial t} = D\nabla^2 \delta C(\vec{r}, t)$$

which can be easily solved by taking a Fourier transform:

$$\delta C(\vec{q}, t) = \delta C(\vec{q}, 0) \exp(-Dq^2 t)$$

The matrix M has just one eigenvalue, $\lambda = -Dq^2$, and its only eigenvector is trivially $X = 1$. Substituting these values into (2-16) yields

$$G(t) = \frac{(2\pi)^{-3}}{Q^2 \bar{C}^2} \int \mathrm{d}^3\vec{q} \, Q^2 \bar{C} \exp\left(-\frac{w_{xy}^2}{4}\left(q_x^2 + q_y^2\right) - \frac{w_z^2}{4} q_z^2 - Dt\left(q_x^2 + q_y^2 + q_z^2\right)\right)$$

$$= \frac{1}{\bar{C}V}\left(1 + \frac{t}{\tau_D}\right)^{-1}\left(1 + \frac{t}{\tau_D'}\right)^{-1/2} \tag{2-17}$$

where $V = \pi^{3/2} w_{xy}^2 w_z$ is an effective sampling volume, and $\tau_D = w_{xy}^2/4D$ and $\tau'_D = w_z^2/4D$ are, respectively, the characteristic times of diffusion across and along the illuminated region.

Finally, denoting the average number of molecules in the sampling volume as $\overline{N} = V\overline{C}$ and the aspect ratio of the sampling volume as $\omega = w_z/w_{xy}$, we obtain

$$G(t) = \frac{1}{\overline{N}}\left(1 + \frac{t}{\tau_D}\right)^{-1}\left(1 + \frac{t}{\omega^2\tau_D}\right)^{-1/2} \tag{2-18}$$

As we could expect, the amplitude of the correlation function is inversely proportional to the average number of molecules in the sampling volume, since the fluctuations $\delta N/\overline{N}$ in the number of molecules in the sampling volume are inversely proportional to $\overline{N}^{1/2}$ and since *G(t)* is second order in the intensity of fluorescence.

In (2-17) and (2-18), each of the directions of translational motion brings in a term like $(1 + t/\tau)^{-1/2}$, so that for a two-dimensional diffusion in the *xy* plane, we have

$$G(t) = \frac{1}{\overline{N}}\frac{1}{1 + t/\tau_D} \tag{2-19}$$

In practice, (2-19) is also a good approximation to a 3D system with the illumination conditions such that $\omega^2 >> 1$ ($\tau_D << \tau'_D$), so that the relaxation of the fluctuations of the number of molecules in the sampling volume is determined by the rate of diffusion in the smaller dimensions.

Thus, the concentration and the diffusion coefficient of a fluorescent species can be evaluated with the help of equations (2-18) and (2-19) from the FCS measurement of *G(t)*, provided the dimensions of the sampling volume are calibrated in a separate experiment.

2.3 FCS in Cellular Studies

Fluorescence correlation spectroscopy (FCS) is the latest addition to biophysical techniques used in conjunction with imaging. Based on a confocal optical setup, similar to a laser scanning microscope (Figure 2-2), FCS relies on different principles than the earlier mentioned techniques and has different advantages and limitations. It is becoming increasingly evident that live cell auto- and cross-correlation can provide new insights into cellular processes previously inaccessible in vivo as is discussed here. Also, some of the pitfalls associated with the use of this technique are highlighted, and strategies to overcome some current limitations associated with in vivo FCS are mentioned.

Whereas in laser scanning microscopy (LSM), statistical fluctuations in the fluorescence intensity from a small detection volume, arising at low concentrations and short integration times, represent an undesired source of noise, these fluctuations constitute the signal in FCS (Figure 2-3) and need to be recorded with high temporal resolution. Although higher concentrations are normally employed in LSM to improve signal quality, a concentration range can generally be found that supports both acceptable quality of visualization in LSM and good FCS fluctuation measurements.

Thus, the use of a combined setup incorporating both techniques is practicable. This combination of FCS with not only classic fluorescence and transmitted light microscopy, but also confocal microscopy in a single setup is very valuable, since it allows for positioning of the FCS measurement volume with better (axial) resolution. Also, recording of the FCS measurement along with a confocal image of the object aids in interpretation of the data.

There are different possibilities for the implementation of a combined LSM and FCS system. One alternative is to have fully separate modules for LSM and FCS

detection, as realized in the commercially available ConfoCor2 system by Carl Zeiss (Jena, Germany). This setup has the advantage that it makes use of the existing highly advanced LSM technology, in which the beam is scanned in the lateral (xy) direction by scanning mirrors, without the need to subject the FCS beam to a passage through these potentially perturbing optical components.

Also, separate detectors can be used, generally photomultiplier tubes (PMTs) for LSM, which can tolerate high photon fluxes without deviations from linear detection characteristics, and avalanche photodiodes (APDs) for FCS, which generally provide a much higher quantum efficiency, but are easily damaged by high light intensities. The disadvantage of this kind of combined system where the LSM beam is scanned by means of mirrors, while the FCS beam is positioned through movement of the sample stage, consists of the fact that the lateral FCS beam positioning accuracy is currently limited to about ±0.3μm. Other, home-built setups use only one beam and one detector (an APD) for LSM and FCS, either by xy-scanning the beam using mirrors[42] or xy-scanning the stage with a piezo drive.[43]

Different methods for evaluating time-dependent fluorescence fluctuations provide access to different parameters. For example, autocorrelation analysis[44-48] is suitable for investigating mobilities, whereas related methods of photon counting histograms[49-51] and similar approaches[52] analyze the fluctuations to obtain information on different brightnesses of species.

Most in vivo applications so far have used correlation analysis applying one of the following definitions of the autocorrelation function:

$$G^{\delta F}(\tau) = \langle \delta F(t) \delta F(t+\tau) \rangle / \langle F(t) \rangle^2 \qquad (2\text{-}20)$$

or

$$G^F(\tau) = \langle F(t)F(t+\tau)\rangle / \langle F(t)\rangle^2 \quad (2\text{-}21)$$

Calculation of the autocorrelation curve may be performed off-line or on-line, by hardware correlator cards or by fast software computation. With online correlation, the resulting curve is conveniently displayed during the measurement, along with a fluorescence trace with low time resolution, which allows visual inspection of the stability of the measurement, i.e., if bleaching or unexpectedly large fluctuations in the count rate are present. For a number of simple diffusion models, fluorescence autocorrelation theory[53,54] yields analytical functions, which are fitted to the measured curves by nonlinear least-squares fitting, a procedure implemented in a number of data analysis packages (e.g., Origin, OriginLab, Northampton, MA) and in the ConfoCor2 system software.

For example, in a system in which one fluorescent species is undergoing free isotropic Brownian diffusion in all three dimensions, the fluorescence autocorrelation curve is fitted to the function

$$G(\tau) = N_{\text{eff}}^{-1}(1 + \tau/\tau_{\text{diff}})^{-1}\left(1 + \tau/(S^2\tau_{\text{diff}})\right)^{-1/2} \quad (2\text{-}22)$$

The structure parameter S characterizes the shape of the ellipsoidal detection volume. The diffusion time, i.e., the average lateral transit time of the particles through the focus, τ_{diff}, relates to the diffusion coefficient by $\tau_{\text{diff}} = \omega_0^2/4D$. N_{eff} denotes the average number of particles residing in the effective measurement volume. Consequently, ω_o, S, and V_{eff} can be determined from a simple calibration measurement with a solution of freely diffusing particles of known diffusion properties, which then allow for

calculation of diffusion coefficients D from characteristic diffusion times τ_{diff} , and of local concentrations from particle numbers N_{eff} .

For large structure parameters S or two-dimensional diffusion, as expected in planar membranes, the equation simplifies to

$$G(\tau) = N_{\text{eff}}^{-1}(1 + \tau/\tau_{\text{diff}})^{-1} \tag{2-23}$$

Fluorescence fluctuations arise not only from diffusion through the focal volume, but also from reversible transitions into nonfluorescent states on a faster time scale (triplet transition,[55] isomerization,[56] reversible protonation,[57] etc.) Therefore, it is usually necessary to include one or more exponential terms in the fitting function, as shown in Figure 2-4.

Fluorescence correlation spectroscopy commonly accesses dynamics on time ranges between 1 μs and 100 ms. For convenient plotting of this very wide dynamic range, a logarithmic time scale is generally used. When analyzing dynamics on the very fast scale (faster than the translational diffusion of small molecules through a diffraction-limited focus, i.e., for instance triplet blinking dynamics or rotational diffusion), special precautions need to be taken to avoid artifacts.

For example artifacts arising from detector afterpulsing depend on the kind of detector being used and can be prevented by splitting the emission light in half, directing it onto two detectors, and computing the crosscorrelation function rather than the autocorrelation functions.

Since FCS temporal resolution is below 100 ns, limitations of FCS for in vivo applications will more likely appear in the slow time range. When analyzing slowly moving molecules, e.g., molecules interacting with the cytoskeleton, nuclear DNA, or

membranes, one has to ensure that acquisition times are sufficiently long to capture the process and, most importantly, that the molecules under investigation are not photobleached during their transit time through the focal volume.

Photobleaching causes an erroneously fast diffusion (since the bleaching of the molecules mimics exit from the focal volume) and the photobleaching decay in the fluorescence trace leads to a decay in the correlation curve[58] which often prevents proper curve evaluation by standard models. Thus, it is rather important to check the influence of the laser power on the fluorescence trace and the correlation curves before recording the actual measurements. Also, one should be aware that the molecule of interest is likely to be less mobile and thus more easily bleached in the live cell than in vitro. In particular, a heterogeneity of diffusing species might be observed in vivo, exhibiting a distribution of mobilities. Thus, if the laser is allowed to illuminate the sample before the start of the data acquisition, a potential immobile fraction can be bleached away. This prebleach is inevitable if the stage is positioned during observation of the fluorescent spot produced by the laser beam in the sample, but it can be avoided if the positioning is carried out ‘‘blindly’’ according to a scanned image (photobleaching during scanning is not biased toward less mobile molecules).

However, the prebleach may also deliberately be used to be able to observe the mobile fraction afterward.[58] Particularly for the slow diffusion encountered in membrane applications, it may be hoped that fluorophores with even higher photostability will lead to an extension of the accessible time range.

Suitable dyes. Whereas in fluorescence imaging, bleaching might easily be avoided by working at lower laser intensities or shorter acquisition times and simply

increasing probe concentration, this is not a solution when doing FCS. In FCS, the signal-to-noise ratio is governed largely by the molecular brightness. Therefore, the setup alignment always needs to be optimized and the fluorophores need to be selected for excellent absorbance, quantum yield, and photostability before being used in an FCS application.

Among the dyes that can be covalently linked to biological molecules via reactive groups, a substantial number have proven useful for FCS experiments. Suitable examples include rhodamine dyes (rhodamine green, tetramethylrhodamine, rhodamine 6G), cyanine dyes (Cy2, Cy3, Cy5), Bodipy and Alexa dyes. The Alexa dyes mentioned may be preferable over the rhodamine dyes for in vivo applications, because they exhibit a lower hydrophobicity.[59] Since in FCS, the fluorescence properties of the single diffusing units are of crucial relevance, the signal is considerably improved by a high labeling ratio, i.e., if one looks at the diffusion of beads, vesicles, or proteins loaded with several dye molecules each. On the other hand, an excessively high labeling ratio may interfere with biological function.

If the labeling is random, there will be species of different brightness. If the brightness distribution function is unknown, this uncertainty impedes correct interpretation of particle numbers (concentrations).

Random labeling of proteins is usually done by aminoreactive labeling procedures. A distinct labeling ratio can usually be achieved in nucleic acid labeling. In protein labeling, distinct labeling ratios of one fluorophore per subunit are achieved if the protein is mutated to have exactly one Cys residue and a thiol-reactive probe is used.

2.3.1 Reliability of Multicomponent Fitting

The large time range accessible by FCS makes it possible to analyze the superposition of various diffusion (and/or blinking) processes that take place on different time scales in a single FCS measurement. Their respective time scales can be revealed by fitting the autocorrelation curve to a multicomponent diffusion model. For instance, the model for two components X_A and X_B with diffusion times τ_A and τ_B reads

$$G(\tau) = N_{\text{eff}}^{-1}\left\{ Y_A(1+\tau/\tau_A)^{-1}\left(1+\tau/(S^2\tau_A)\right)^{-1/2} + Y_B(1+\tau/\tau_B)^{-1}\left(1+\tau/(S^2\tau_B)\right)^{-1/2}\right\} \quad (2\text{-}24)$$

where Y_A and Y_B represent the fractions of components X_A and X_B, respectively.

Due, however, to the nature of the hyperbolic decay of the obtained correlation curves, the diffusion of multiple species can be resolved only if their diffusion times are well separated. Computer simulations[60] show that for good signal quality this could in principle be achieved if $\tau_A = \tau_B$ equals at least 1.6, but for worse signal and more disparate fractions, a two-component fit may not be justified even for $\tau_A/\tau_B = 10$ (Y_B = 0:1).[60] Care has to be taken in interpreting results from multicomponent fits, since invoking too many parameters may seemingly improve the fit without providing reliable parameter values. When fitting a two-component diffusion in the case where one of the components exists only in a low fraction, the fit results for these fraction parameters are often biased toward values closer to each other than the expected values. Since some parameters in the model equations are strongly interdependent (correlated), it is helpful if calibration and control measurements are done and as many parameters are fixed as possible. Usually, the structure parameter, which describes the shape (elongation) of the detection volume and is interdependent with the diffusion time, needs to be determined beforehand in an in vitro calibration measurement of free dye. Also, if each species can

be measured separately, diffusion times can be fixed in a multicomponent fitting procedure.

2.3.2 Limitations of Autocorrelation Analysis for *In Vivo* Binding Experiments

A number of binding experiments have been performed in vitro, based on the change in diffusion time.[61-65] However, this kind of measurement is limited to cases with a considerable change in molecular mass on binding (binding of a small fluorescent ligand to a larger macromolecule) since the diffusion time scales only with the third root of the molecular mass.

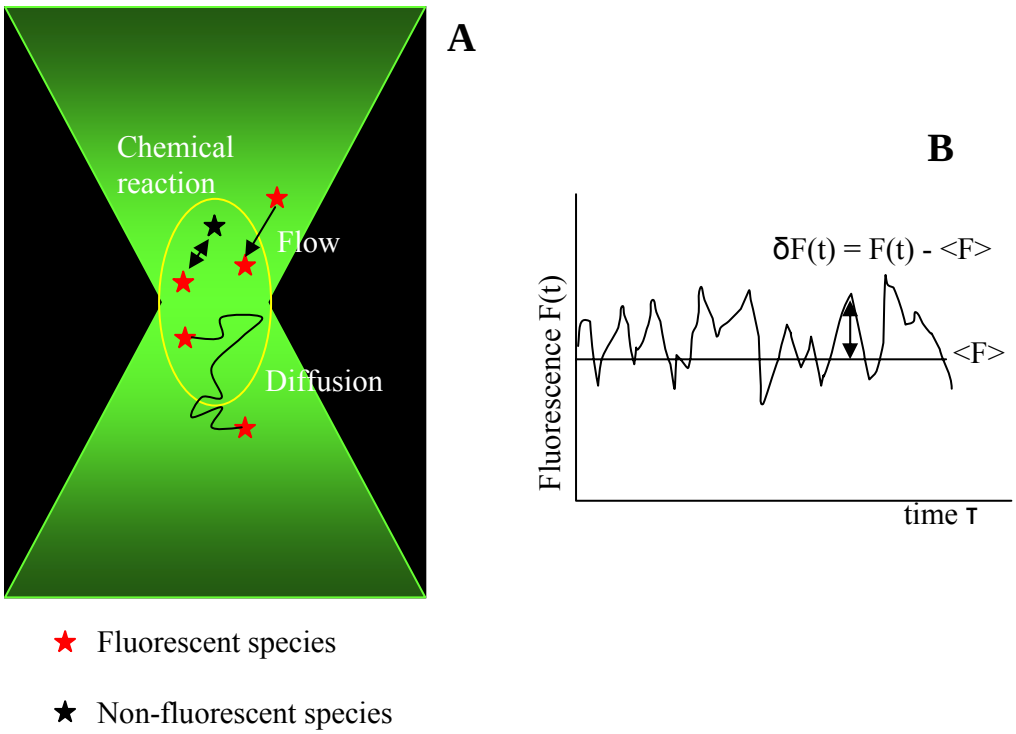

Figure 2-1. The principle of FCS. (A) Fluorescent molecules, at equilibrium, diffuse or flow though a volume element or undergo transitions between different fluorescent states. (B) These processes lead to fluctuations δF(t) in the measured fluorescence signal F(t) from the average fluorescence <F>.

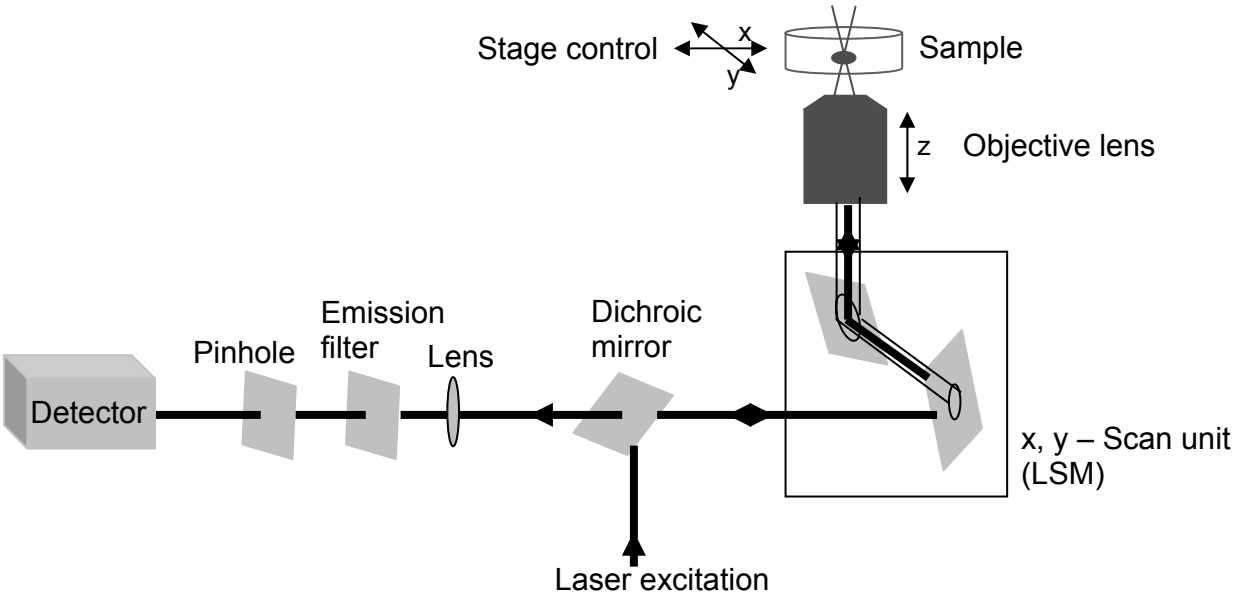

Figure 2-2. Optical setup used in laser scanning microscopy (LSM) and fluorescence correlation spectroscopy (FCS). Both optical techniques use a confocal setup, usually based on an inverted microscope: The parallel laser light from one or two lasers is reflected onto the back aperture of the objective. Homogeneously illuminating the back aperture of the objective results in a diffraction-limited excitation volume in the sample. The Stokes-shifted fluorescence light from the sample passes straight through the main dichroic mirror and is focused onto a pinhole and detected by a photomultiplier tube (PMT) or avalanche photodiode (APD). For good axial resolution, high-NA objectives need to be employed. Since buffer solutions and live biological samples are water-like, water immersion is preferred to minimize aberrations. In the case of LSM image acquisition, the excitation volume is scanned laterally (x–y) through the sample, either by using scanning mirrors to deflect the beam or by moving the sample. In contrast, for normal FCS measurements, the FCS spot is positioned before the measurement and then kept stationary in the sample during data acquisition.

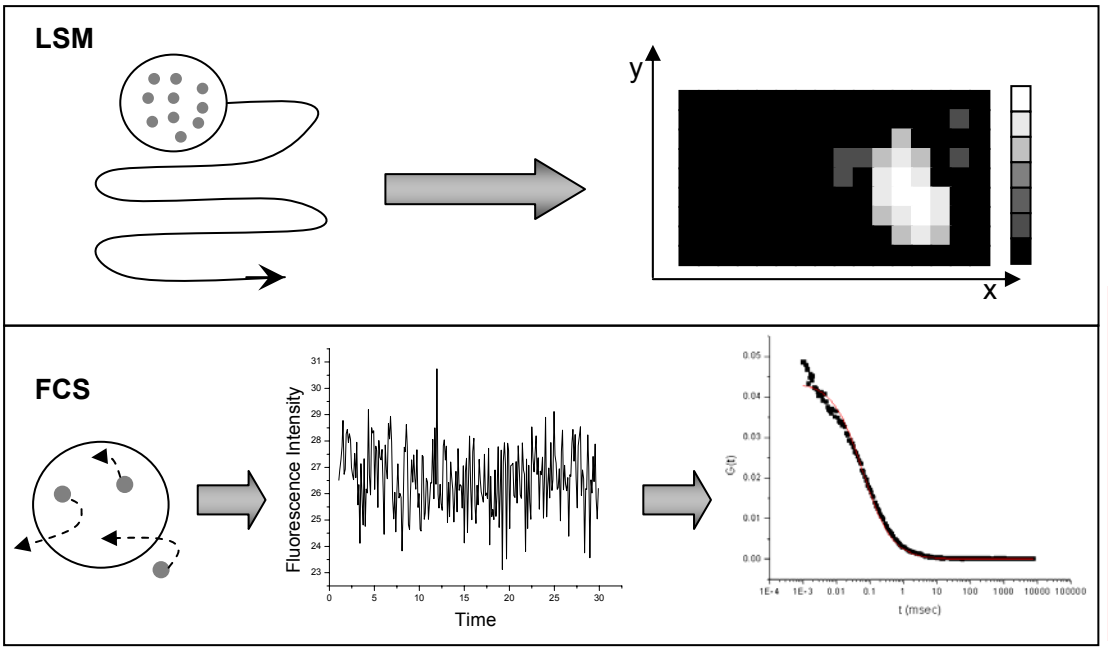

Figure 2-3. Acquisition and processing of the fluorescence signal in laser scanning microscopy (LSM) and fluorescence correlation spectroscopy (FCS). In LSM, the total fluorescence from the confocal detection volume is recorded. Low fluorophore concentrations along with short integration times (high-speed scans, high-resolution scans) only lead to undesired noise due to statistical fluctuations of the number of fluorophores in the detection volume. In contrast, in FCS, the statistical fluctuations of fluorophores in the small confocal detection volume constitute the measurement signal. Thus, low concentrations and bright fluorophores are required to obtain an FCS signal. However, in *in vivo* measurements, fluorophore concentrations should not be too low, as the fluorescence signal needs to be considerably above the background, arising for instance from cellular auto-fluorescence and scattering. The fluorescence fluctuations are mathematically processed using an autocorrelation algorithm. The resulting autocorrelation curve is interpreted by fitting to equations that have been derived for different diffusion models. In simple cases, the number of fluorophores in the detection volume can be read from the reciprocal of the amplitude and the diffusion time from the half-value decay of the autocorrelation curve. From these parameters, the concentration and the diffusion coefficient of the labeled particles can be calculated, if a simple in vitro calibration measurement with a dye solution has also been performed.

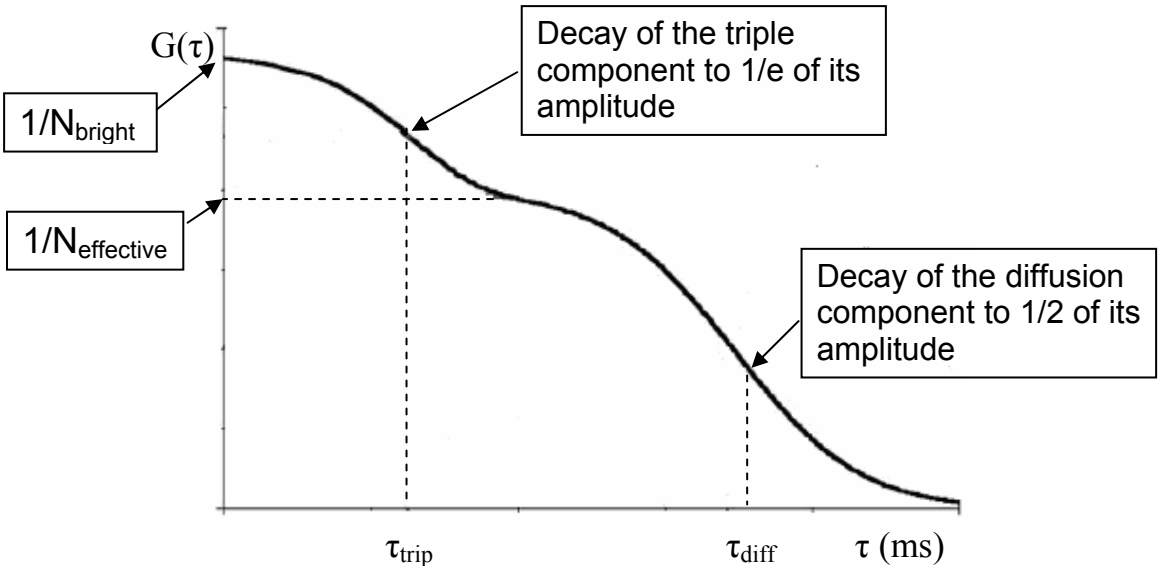

Figure 2-4. Parameters in a simple autocorrelation curve. Computed fluorescence correlation curve for two-dimensional diffusion including triplet blinking. The reciprocal of the number of particles in the detection volume determines the amplitude of the FCS curve; the kinetics of the triplet blinking process (relaxation time strip) and the particle mobility (diffusion time τ_{diff}) determine the two characteristic decays in this curve.

CHAPTER 3
BUILDING AND TESTING OF THE FCS SET-UP

3.1 The Standard Confocal Illumination and Detection Scheme

As follows from the theoretical discussion, the FCS measurement requires small sampling volumes (to ensure a small number of molecules and, hence, a high amplitude of correlation function), as well as high photon detection efficiency and good rejection of background fluorescence.

In a confocal setup (Figure 3-1) the excitation laser light is directed by a dichroic mirror into a high-power objective, which focuses the light inside the sample. The fluorescence emission is collected through the same objective and focused onto a pinhole, so that the laser beam waist inside the sample is imaged onto the pinhole aperture. The conjugation of the objective and the pinhole creates a spatial filter, which efficiently cuts the sampling volume to a diffraction limited size. After the pinhole, the fluorescence signal can be collected directly by a photon counting detector and processed into an autocorrelation function.

3.2 Components of the Set-up

3.2.1 Excitation

Lasers. The most crucial part of the FCS experiment is efficient detection of fluorescence from a microscopic ‘‘probe’’ volume.[66] This can be achieved by using tightly focused illumination (with a high-numerical-aperture objective lens) and confocal detection. For multiphoton excitation, focused illumination by itself ensures a small probe volume irrespective of the detection setup. The absolute value of the diffusion coefficient *D*, if required, can be extracted from the data only if the shape of the illumination volume is known. Lasers are the perfect light sources for FCS as the focal volume can be reduced to a fraction of a femtoliter. A well characterized laser beam also allows reliable estimation of the focal volume. Lamps are not

suitable light sources for FCS. For single-photon experiments, low-power (~1mW) continuous-wave lasers are sufficient.[67] In our set-up we incorporated an Ar^+-laser and we used neutral density filters to attenuate the beam intensity from 20 mW down to 1.2 mW.

Smaller spot size at the focus requires a larger beam diameter at the back aperture of the objective lens, implying that an expansion of the laser beam is usually necessary. The smallest focal volume is achieved by overfilling the back aperture of the objective lens. The focus thus achieved is nearly diffraction limited, but the focal plane intensity distribution is not described by a simple analytical function.[68] A Gaussian intensity distribution at the focal plane can be obtained by underfilling the back aperture of the microscope objective but this yields a slightly larger observation area for the experiment. In order to achieve a Gaussian beam with as small a focal volume as possible we only slightly underfilled the objective back aperture, as shown in Figure 3-2.

An important issue when focusing a laser through a high-numerical aperture objective and detecting through the same objective is the refractive index of the sample. Focusing and detection will be optimal only if the sample's refractive index exactly matches that of the objective's immersion medium. A water immersion objective is usually for solution measurements so that the immersion medium's refractive index is assumed to be 1.33 (Figure 3-2). However, when performing FCS in living cells, the refractive index of the sample may be as high as 1.38. The refractive index mismatch introduces slight aberrations into the laser focusing and the confocal fluorescence detection,[69] and leads additionally to a slight offset of center of focus and center of detection along the optical axis. Both effects lead to an apparently larger detection volume and thus an apparently smaller diffusion coefficient. However, the error that is

introduced by the refractive index mismatch remains below 12 % up to a sample's refractive index of 1.38. This is still within the accuracy range of most FCS measurements.

Cover slide thickness. When working with water immersion objectives, coverslide thickness plays a crucial role. All water immersion objectives are correctly imaging only for one specific thickness value. Most state-of-the art objectives provide correction rings for adjusting them to changing values of actual cover-slide thickness.[70]

The quality of the autocorrelation curve is no measure for correct cover-slide thickness. All curves are fitted well by the reference curve, but yield different apparent values of the diffusion coefficient. Thus, for each cover-slide used in a real experiment, it is crucially important to precisely readjust the water immersion objective to the actual cover slide thickness value.

Fluorescent dyes. An FCS measurement relies on the fluorescence of the compound under study, this fluorescence being either natural, or, more generally, resulting from specific dye-labeling of the compound of interest. While there is a huge variety of dyes commercially available for fluorescence microscopy, not all of these dyes would perform well in an FCS experiment.[71]

The quality of the measurement is determined by the fluorescence emission per molecule. Thus, the dye has to be bright, i.e. it must be characterized by high extinction coefficient and high quantum yield. Next, different deficiencies of the dyes must be avoided. The fluorescence emission is proportional to the excitation at low laser intensities only. At high intensities the dye emission saturates because of two reasons.[72] First, the emission of the dye is limited to one photon per residency in the excited state (whose lifetime is typically in the range of few nanoseconds). Thus, it cannot be better than 10^8 photons s^{-1}. Second, even before reaching this limit, the fluorescence of the dye saturates because of trapping in a non-fluorescent triplet state.

The triplet state not only limits the emission, but also shows up in the correlation function in the microsecond range concealing other processes which might be occurring with the labeled molecule in this time range. Finally, upon prolonged illumination the dyes can be bleached irreversibly. While normally this is not a problem for FCS measurements on mobile molecules (their diffusion time across the sampling volume is short, typically 100 μs, compared to the bleaching time), the photobleaching is of concern for the experiments on immobile or slowly moving objects.[71] Currently the dyes which comply best with these requirements are the derivatives of rhodamine, and we used rhodamine 123 for set-up calibration. While fluorescein is not one of the best choices for FCS experiments, we rarely observed any photobleaching of the fluorescein isothiocyanate-labeled aptamer within the 30-second measurements.

3.2.2 Collection

The fluorescence from the sample is collected using the same microscope objective lens that is used for excitation. This ‘‘epifluorescence’’ geometry automatically ensures that the collected fluorescence is decoupled from the forward-moving excitation light.

For the best collection of fluorescence, high power objectives are used. Oil-immersion objectives are characterized by the highest numerical aperture (NA ~ 1.4). However, they are designed to focus and collect light in a high refractive index environment (that of the immersion oil or of the cover glass), such that their optical quality is reliable only when the focal plane is right at the surface of the cover glass. Focusing the laser excitation deeper inside aqueous samples (typically more than a few microns from the glass–water interface) generates optical aberrations as well as sub-optimal fluorescence collection, which can jeopardize the quality of an FCS measurement.[73] This problem, well known in confocal microscopy, is solved through the use of water-immersion objectives. Although the numerical aperture of these objectives (NA ~ 1.2) is smaller than that of the oil-immersion ones, for experiments with aqueous samples, water-

immersion objectives have a clear advantage of focusing the excitation light and collecting the emission efficiently. In our set-up we used a 60x water immersion objective with N.A. = 1.2.

3.2.3 Filters

The collected fluorescence needs to be separated from the excitation light path, and directed to the detector. A dichroic, which is a specially coated thin optic that transmits one range of wavelengths while reflecting another range, is used for this purpose. Remaining excitation photons and other stray photons are filtered out by a bandpass interference filter, which is another specially coated optic designed to transmit light only within a small wavelength window. These two filters need to be chosen carefully to effectively cut off the excitation light and reduce the nonspecific background, while maximizing the transmission of the fluorophore emission to the detector.

3.2.4 Pinholes

The filtered fluorescence is focused onto a pinhole in the image plane. Light originating from the focus passes through the pinhole aperture, while light from other regions is preferentially blocked. The probe volume in FCS experiments is a convolution of this detection profile with the illumination profile at the focal spot.[74] The most convenient way of introducing a pinhole in the instrument is focusing the fluorescence onto a multimode fiber where the fiber face acts as the pinhole. Changing the fiber allows easy alteration of the pinhole aperture size without the need for substantial realignment of the instrument.

The best signal-to-background values are obtained with pinholes of the size of the image of the laser beam waist in the plane of the pinhole. We used a multimode optical fiber with a 50 μm internal diameter.

An important issue of any FCS measurement is the perfect alignment of the detection optics, in particular the adjustment of the pinhole position along the optical axis. Whereas off-

axis pinhole alignment is relatively easy to achieve, due to the quick fall-off of the detectable fluorescence intensity with increasing lateral displacement away from the optical axis, precise adjustment of the pinhole position along the optical axis is much more difficult to control. The increasing pinhole misplacement leads to a decreasing overlap between excitation focus and center of the collection efficiency function, thus apparently enlarging the detection region and resulting in a slower fall-off of the autocorrelation. Unfortunately, it is not possible to judge the pinhole position by the quality of the autocorrelation curve.[75] All obtained autocorrelation curves can be well fitted by the reference curve, yielding apparently meaningful fits but increasingly larger diffusion coefficients. However, significant deviations of the apparent value of the diffusion coefficient from its true value occur only for rather large pinhole misplacements. The situation becomes more critical for objectives with increasing numerical aperture, for example when using an oil immersion objective with 1.4 NA. Nonetheless, if one uses the same pinhole position for measuring the reference and the probe sample, correct ratios of diffusion coefficients can be derived regardless of the absolute pinhole position.

3.2.5 Detection of the Fluorescence

The preferred detector for FCS experiments is a sensitive single-photon counting avalanche photodiode (APD) module. Photomultiplier tubes (PMTs) can also serve that purpose. However, in the visible range of wavelengths an APD is a better detector than a PMT. The peak quantum efficiency of an APD is >60% whereas that of a PMT is typically ~20%.[76-79] Use of a fiber-coupled APD makes the alignment and the light shielding of the instrument simpler. In the UV range of wavelengths the APD has lower sensitivity and a PMT may be a better option.

In our set-up we used the single-photon counting APD module SPCM-AQR-14 from Perkin Elmer with a photon detection efficiency of ~55% at 520 nm.

3.2.6 Correlators

We are using a hardware multiple tau digital correlator (ALV 5000/EPP, ALV-GmBH, Langen, Germany) with 100% real time correlation from the initial 125 ns on.

3.3 Construction of the Set-up

The instrument is constructed by assembling commercially available optics and optic holders into a rigid framework on an optical bench.

A continuous-wave Ar^+ laser (Figure 3-3) is used as the light source. The laser beam is routed through two mirrors and expanded to a diameter of ~10 mm using a beam expander. The expander is made up of a plan-concave lens and a plan-convex lens of focal lengths -5 and 10 cm, respectively. The distance between the lenses adds up to the sum of their focal lengths to ensure proper beam collimation. A filter wheel containing a series of neutral density filters is placed in the excitation beam path so that the intensity of the excitation light can be easily adjusted. The expanded beam is reflected by two other mirrors and enters the back port of an Olympus IX70 inverted microscope (Figure 3-4). Here, the laser beam is reflected by the dichroic mirror held inside the slider box of the microscope, and is then focused into the sample through a microscope objective lens. The fluorescence from the sample is collected by the same microscope objective lens used for excitation and is separated from the excitation light by the dichroic mirror, which now passes the fluorescence. The filtered fluorescence is focused by the tube lens of the microscope, is reflected by a prism reflector, and exits through the side port with a focus close to the body of the microscope. The signal is then filtered with a bandpass emission filter and focused onto a multimode fiber. The fiber front face works as the pinhole and the fiber holder allows translation along the radial (x and y) directions and axial (z) direction. The fiber is coupled to a single photon counting module SPCM which detects the signal. The detector sends the signal to the input channel of the hardware correlator.

3.4 Test Experiments

Once the instrument is set up and aligned, several test experiments are performed to characterize it. A stable dye of known value of the diffusion coefficient is used to estimate the probe volume. Regular FCS measurements are done for this standard sample to keep track of any change of alignment.

To verify if the instrument is working properly, two sets of standard experiments were performed: FCS measurements of solutions with different concentrations of a suitable dye, and measurements with fluorescent-labeled molecules of different molecular weights and same concentration.

3.4.1 Varying Dye Concentration

Figure 3-5 shows the autocorrelation function measured for rhodamine 123 at different concentrations of the dye. The increase in the number of molecules N is proportional with the increase in concentration, as expected.

3.4.2 Varying Molecular Weight

Figure 3-6 shows the molecular weight dependence of the autocorrelation function of 5 μM fluorescein-dextran complexes. Increased molecular weight makes the molecules diffuse slower, which is reflected in a shift of the characteristic decay times of the autocorrelation functions to longer delay times.

3.5 Summary and Conclusions

An FCS set-up with single-molecule detection sensitivity was successfully built. The test measurements prove that the system is able to detect very low dye concentrations and distinguish between labeled molecules of different molecular weight.

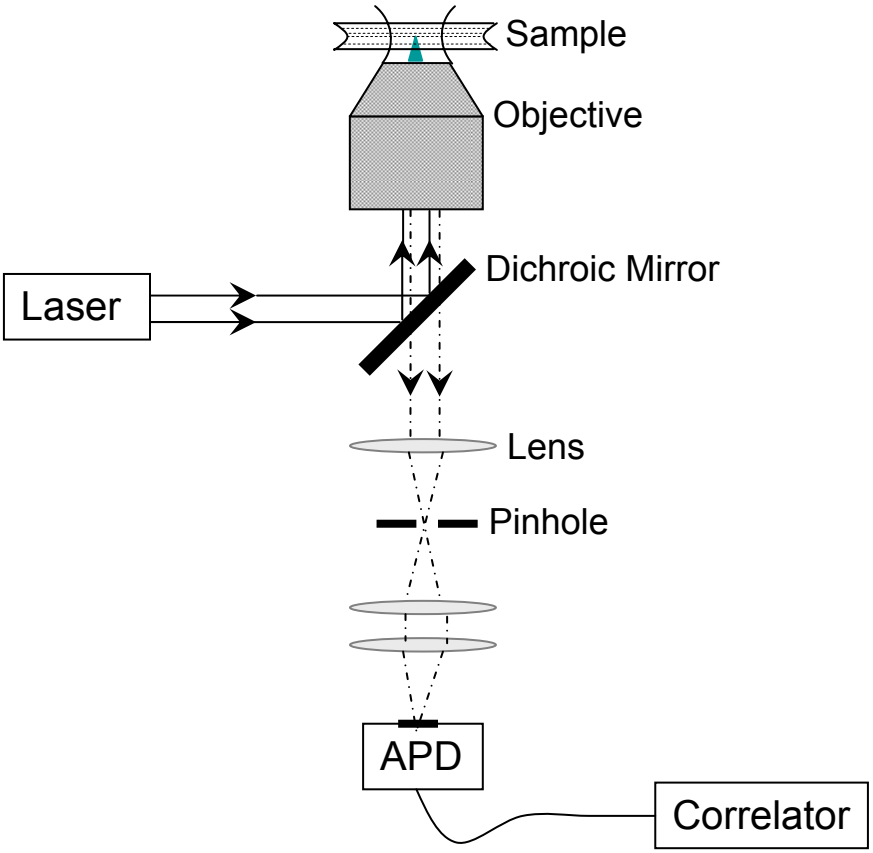

Figure 3-1. Scheme of a standard confocal experimental setup for FCS. The excitation light coming from a laser source is focused onto the sample by the means of a microscope objective. A dichroic mirror is used to reflect the excitation beam entering the back aperture of the objective and to transmit the fluorescence coming from the sample. The fluorescent light is further focused by a lens onto a pinhole and detected by a avalanche photodiode. The signal coming from the detector is processed by a correlator.

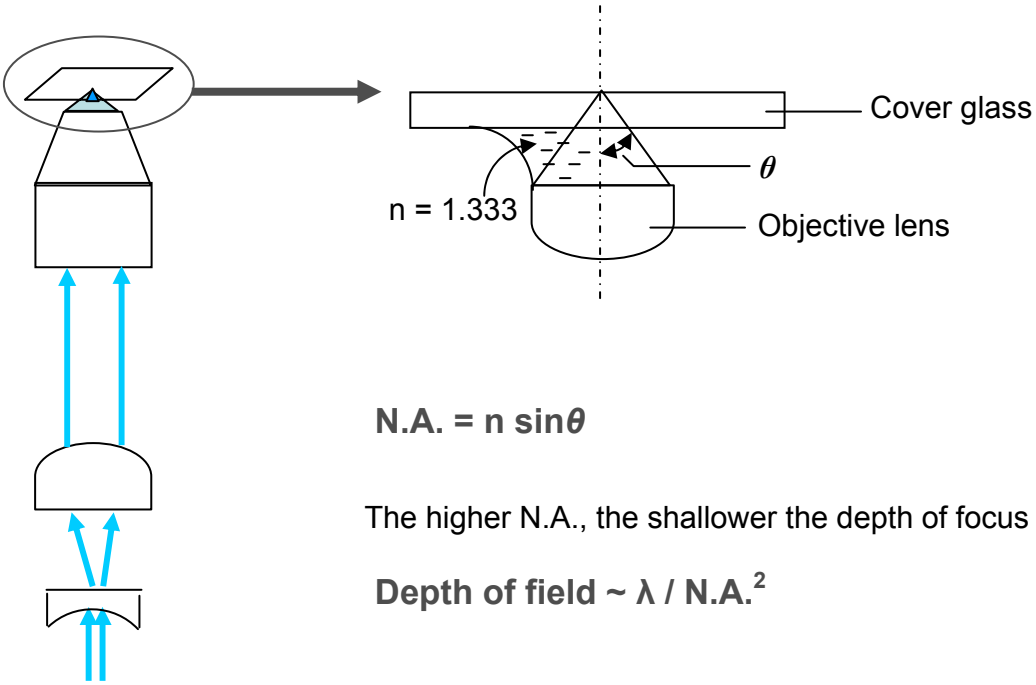

Figure 3-2. Choosing the degree of filling of the back aperture of the microscope objective. To achieve a small confocal volume, a very important parameter to be adjusted was the numerical aperture (N.A.) of the objective lens. A water-immersion objective has been chosen so that the index of refraction (n) is larger than the one for air, but it does not introduce the aberrations that are often observed with an oil medium. A conveniently large half-angle θ of the maximum cone of light that exits the objective lens was obtained by completely filling the back aperture of the objective lens.

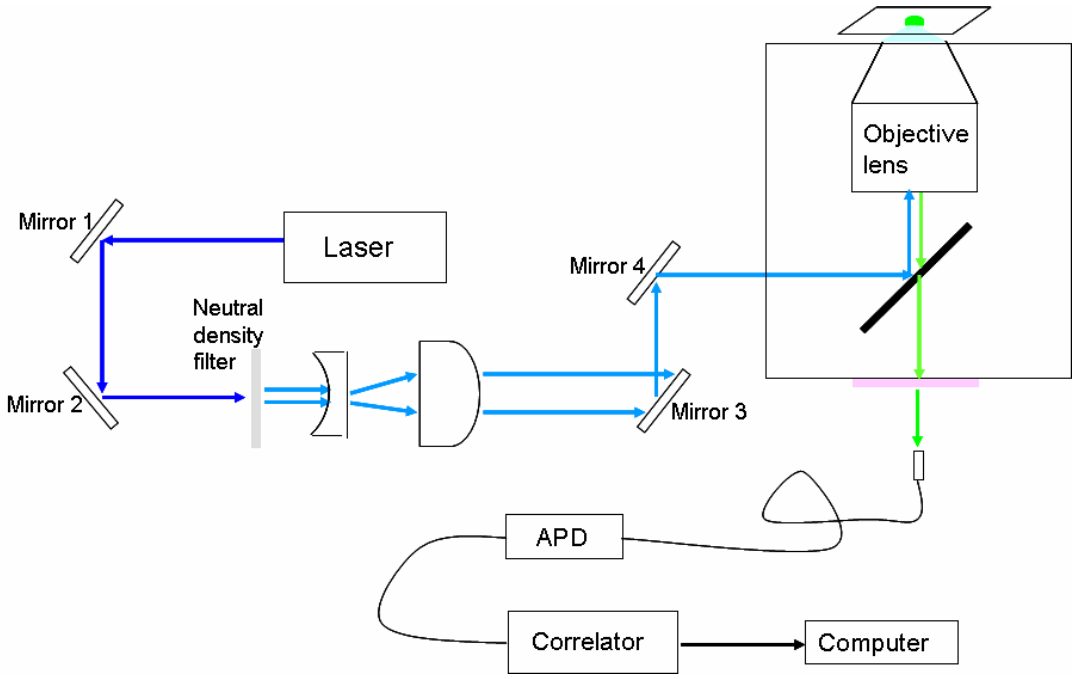

Figure 3-3. FCS instrumental set-up. The light coming from an Ar^+ is routed through two mirrors and expanded by a beam expander, which was made up of a plan-concave lens and a plan-convex lens. The intensity of the excitation light was attenuated by a neutral density filter. The expanded beam is reflected by two other mirrors and enters the back port of an inverted microscope, where the laser beam is reflected by a dichroic mirror, and is then focused into the sample through a microscope objective lens. The fluorescence from the sample is collected by the same microscope objective lens. The filtered fluorescence is focused by the tube lens of the microscope, and exits through the side port with a focus close to the body of the microscope. The signal is then filtered with a bandpass emission filter and focused onto a multimode fiber, which works as a pinhole. The fiber is coupled to a single photon counting module SPCM which detects the signal. The detector sends the signal to the input channel of the hardware correlator.

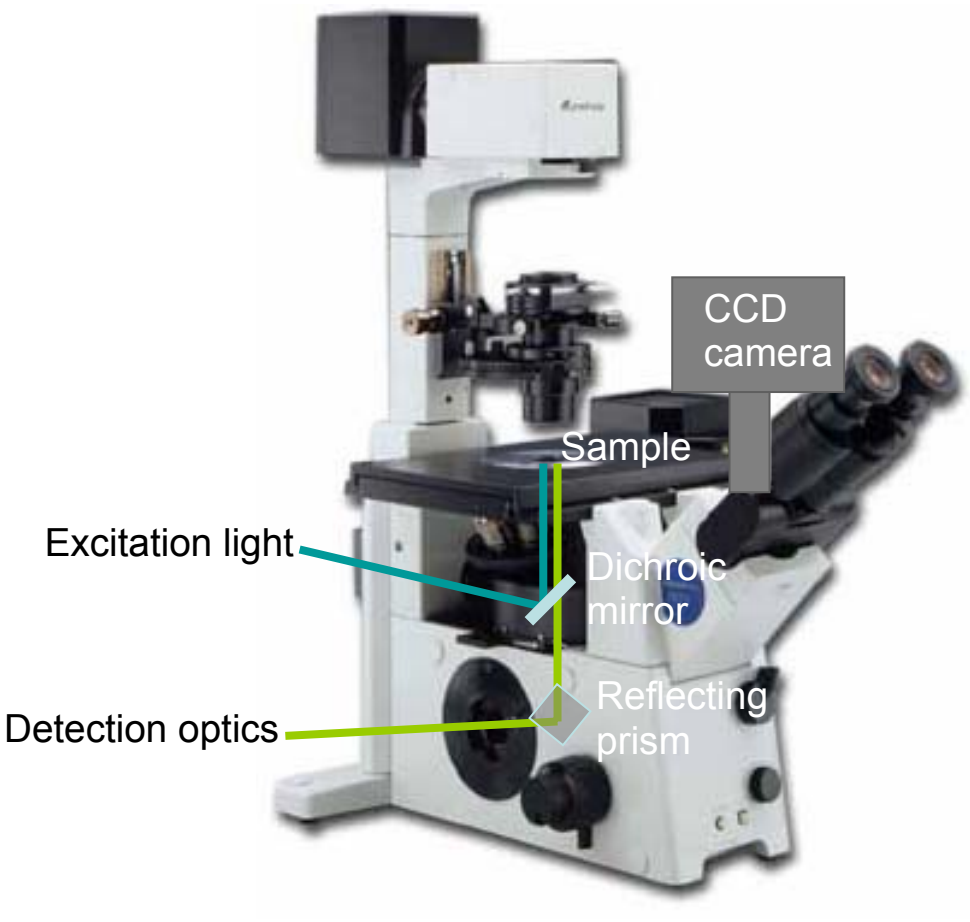

Figure 3-4. Schematic diagram of the FCS instrument incorporated into a fluorescence microscope. The excitation light enters the back port of an Olympus IX70 inverted microscope. Here, the laser beam is reflected by the dichroic mirror held inside the slider box of the microscope, and is then focused onto the sample through a microscope objective lens. The fluorescence from the sample is collected by the same microscope objective lens used for excitation and is separated from the excitation light by the dichroic mirror, which now passes the fluorescence. The fluorescence signal is reflected by a prism reflector, and exits through the side port, where it enters the detection optics.

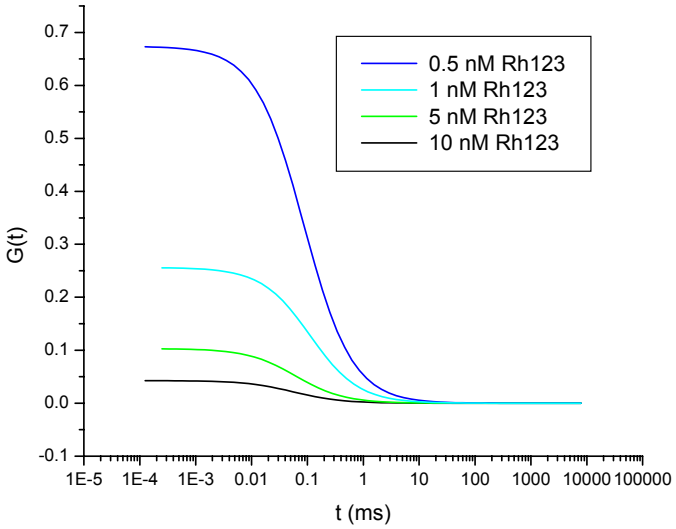

Figure 3-5. Autocorrelation curves of aqueous solutions of rhodamine 123 at different concentrations. The amplitude of the autocorrelation function decreases with increasing dye concentrations.

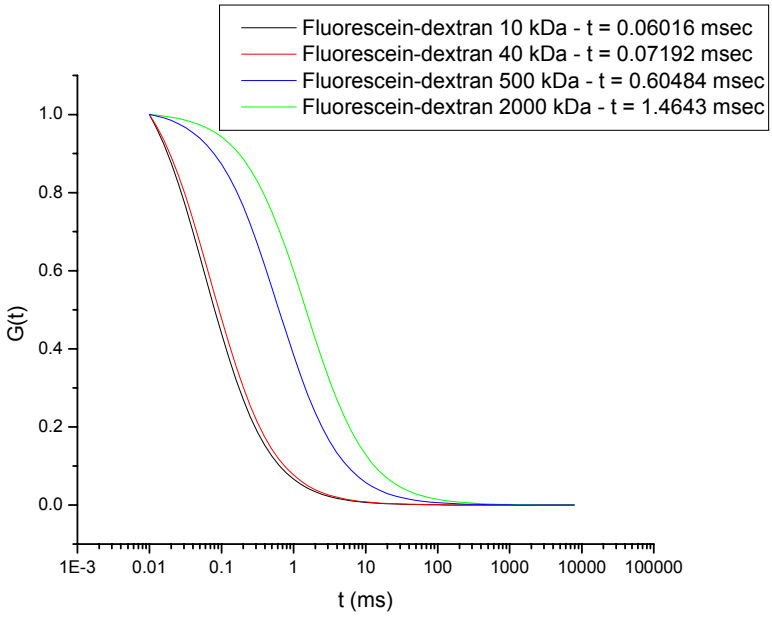

Figure 3-6. Normalized autocorrelation curves of aqueous solutions of fluorescein-labeled dextran of different molecular weights. The diffusion time increases with increasing molecular weight of the fluorescent molecules.

CHAPTER 4
APTAMER BINDING TO CANCER CELLS: DETERMINATION OF THE DISSOCIATION CONSTANT

4.1 Introduction

More than 50 different chemotherapy drugs are available to treat cancer. All of them kill cancer cells, though they work in different ways. All the drugs are designed to go after chemical substances within cancer cells and to interfere with cellular activity during specific phases of the cells' growth cycles. In the process, chemotherapy drugs also kill healthy cells, and that is why side effects develop. Of course, not all drugs work well for all cancers, and in many cases, a combination of chemotherapy drugs is the best course of treatment.

Antibody-based therapies are aimed at molecular targets and they attack cancer cells, sparing most normal cells. Currently, antibody-based agents are used to treat breast cancer, colon cancer, lung cancer, lymphoma, and several types of leukemia, but additional targeted therapies are being developed. Aptamers have been isolated and identified for the recognition of molecular differences expressed on the surface membranes of two different types of cells. These probes can be used to specifically detect target cancer cells based on molecular characteristics in the presence of other cells, leading to effective disease studies and early diagnosis.

4.2 Materials and Methods

Cell lines. BNL 1ME A.7R.1 and BNL CL.2 (mouse hepatoma cell lines) were obtained from American Type Culture Collection. The cells were cultured in Dulbecco's modified Eagle's (American Type Culture Collection) medium with 10% fetal bovine serum (Invitrogen, Carlesbad, CA) and 0.5 mg/ml Penicillin-Streptomycin (American Type Culture Collection, Manassas, VA) at 37^{o}C under a 5% CO_2 atmosphere. The cells were washed before and after incubation with Dulbecco’s phosphate buffer (Sigma) with 5 mM $MgCl_2$. The aptamer solutions were prepared in the same buffer.

Aptamers. The aptamers used were TLS1c (5'- ACA GGA GTG ATG GTT GTT ATC TGG CCT CAG AGG TTC TCG GGT GTG GTC ACT CCT G-3'), TLS9a (5'- AGT CCA TTT TAT TCC TGA ATA TTT GTT AAC CTC ATG GAC-3') and TLS11a (5'- ACA GCA TCC CCA TGT GAA CAA TCG CAT TGT GAT TGT TAC GGT TTC CGC CTC ATG GAC GTG CTG-3'). All the aptamers were selected, synthesized and HPLC-purified in our lab. They were used both in a non-labeled form and labeled with fluorescein isothiocyanate (FITC).

Binding assay. Binding studies were carried out on cells cultured in eight-well Nunc chambers (Nalge Nunc Inc., IL, USA) at 4 °C. Prior to the experiments, cells were washed 5 times with Dulbecco's phosphate buffer saline (Sigma) with 5 mM $MgCl_2$ and incubated with aptamer solutions. Aptamer binding was measured after 40 min incubation of the cells in the presence of 1-40 nM fluorescein isothiocyanate (FITC)-labeled aptamer. Specificity of the aptamer binding was demonstrated by the competitive displacement of the bound FITC-aptamer from the cell surfaces after addition of 1000-fold non-labeled aptamer.

FCS instrumentation. FCS measurements were performed on a custom apparatus, which had been developed from an Olympus IX70, as described in Chapter 3. Briefly, the excitation light of a 488 nm line of an Ar-ion laser was focused onto the sample through a Olympus 60x numerical aperture 1.2 objective for water immersion. The fluorescence was collected by the same objective, separated from the excitation light by a dichroic mirror, then split by a 50/50 cube splitter and sent onto an avalanche photodiode (SPCM-AQR-14, Perkin Elmer) by the means of a 50 μm-inner diameter optical fiber after passing through a 515–555 nm bandpass filter. The sample was illuminated with an excitation power of 20 μW at the back aperture of the objective. The measurements were performed in a volume element of 0.4 fL with halfaxes ω_{xy} = 0.22 μm and ω_z = 1.56 μm. Autocorrelation was processed by a hardware correlator (ALV

5000/EPP, ALV-GmBH, Langen, Germany). Data fitting was performed with MicroCal Origin using a least-square fit algorithm.

Determination of proper illumination intensities. A general concern in FCS systems, but prevalently for applications with slow-moving particles in membranes, is the risk of artificially reducing the dwell time by photobleaching the molecules at high powers. For this reason, we have to work at illumination power levels of less than 100 μW. It is verified that for the applied intensities no photobleaching-related artifacts to the correlation curve. For the measurements that follow, the chosen power is ~20 μW.

4.3 Results and Discussion

The system was first calibrated with Rhodamine 123, as shown in Figure 4-1. The radius in the radial direction was ω_{xy} = 0.22 μm and the radius in the axial direction was ω_z = 1.56 μm. The calculated observation volume was 0.44 fL.

Receptor binding can be analyzed on the basis of the fluorescence intensity autocorrelation function as given in equation 4-1.

$$G(\tau) = \frac{1}{N}\left[\left(1 - \sum s \right)\left(\frac{1}{1+\frac{\tau}{\tau_D^f}}\right)\left(\frac{1}{1+\left(\frac{\omega}{z}\right)^2\frac{\tau}{\tau_D^f}}\right)^{\frac{1}{2}} + \sum s \left(\frac{1}{1+\frac{\tau}{\tau_D^b}}\right)\right] \qquad (4\text{-}1)$$

where $\sum s$ is the bound fraction of the aptamer, (1-$\sum$s) is the fraction if the unbound aptamer, τ^f_b is the diffusion time of the free aptamer, and τ^b_b is the diffusion time of the bound aptamer.

In FCS measurements fluorescence intensity fluctuations are recorded from only those molecules that diffuse through the confocal laser volume element. The time required for the passage of fluorescent molecules through the volume element is determined by the diffusion coefficient, which is related to the size and shape of a molecule. Thus, diffusion times obtained from the analysis of fluorescence intensity fluctuations with autocorrelation functions allow

differentiating faster diffusing and slower diffusing molecules and thus, it is possible to distinguish free ligands from ligand–receptor complexes. In binding studies with the FCS technique, a mixture of several ligand–receptor complexes (components) with different molecular weights and corresponding different diffusion times can be analyzed without any need to physically separate unbound components from bound ones.

When a new technique is applied to study ligand binding, it is necessary to fulfill all the criteria of ligand-receptor interactions such as affinity (the ligand and receptor have affinity for one another), specificity (receptors show specificity in their interactions with ligands), concentration dependency (ligand-receptor interactions are concentration dependent, leading to a binding curve) and reversibility (ligand-receptor interactions are reversible, leading to a dissociation curve). In order to highlight ligand-receptor interactions on live cells (cell cultures) using FCS with reference to the fundamental criteria of ligand-receptor interaction, the interaction between the aptamers selected for liver cancer cells and their receptors will be demonstrated. It is very important to take background fluorescence into account for the judgement of the specific ligand-receptor interaction in live cells when a ligand is tagged with a fluorescent dye.

Background fluorescence usually originates from endogenous proteins if their excitation wavelength is close to that of the dye used. The endogenous proteins such as NADH and FAD produce autofluorescence in blue-green range. Fluorescence signals will be overestimated if they are not corrected for background fluorescence. In order to check background fluorescence the autofluorescence is to be measured in cells without addition of fluorophore labeled ligands. The autocorrelation function of the cell membrane autofluorescence is shown in Figure 4-2, and it

was found to be similar for both cell lines considered in this study. The signal could not be correlated, hence no correction for autofluorescence had to be made.

The laser was focused on the cell membrane, as depicted in Figure 4-3, and fluorescence fluctuations due to both free diffusion and bound labeled aptamer within the measurement volume were correlated.

From autocorrelation curves of the free labeled aptamers, we found the corresponding diffusion times, as shown in Figure 4-4.

In order to observe the binding of aptamers and to check that the aptamer binding is concentration-dependent and it reaches saturation, the liver cancer cells were incubated with different concentrations of FITC-labeled aptamer for 40 min on ice and then we performed the FCS measurements. The intensity autocorrelation function $G(\tau)$ of the aptamer bound to a cell membrane is shown in Figure 4-5. Increasing concentrations of the aptamer led to an increased proportion of aptamers bound to receptors, until saturation was reached. A certain fraction of the unbound aptamer is also observed at the cell surface since the volume element extends into the space above the cell membrane. From the FCS curve fitting, keeping the diffusion times for the free aptamers fixed, we obtain the bound fraction *s* of the aptamer. The binding curve was made by plotting the fraction bound vs. ligand concentration (Figure 4-6). The K_D values for the three aptamers tested were similar to the ones obtained by flow cytometry as shown in Table 4-1.

To check that the aptamer binding to the cell membranes is not only ligand concentration dependent and saturable but also specifically displaced by non-labeled aptamer, we studied the binding in the presence of a 1000-fold molar excess of non-labeled aptamer. The cells were incubated with FITC-labeled aptamer, and binding was measured after 40 min of incubation, as a control. The non-labeled aptamer was then added to the cell culture and dissociation of the

labeled molecules from the cell membrane was observed with time course. As shown in Figure 4-7, the presence of non-labeled aptamer in cells resulted in a drop of FITC-labeled aptamer binding, which was almost entirely displaced after 3 h of incubation with large excess of non-labeled aptamer.

Table 4-1. Dissociation constants obtained for the aptamers selected for liver cancer cells.

Aptamers	**K_D from flow cytometry (nM)**	**K_D from FCS (nM)**
TLS 1c	9.8±0.3	10.0±0.2
TLS 9a	7.4±0.3	8.1±0.2
TLS 11a	4.5±0.4	5.3±1.4

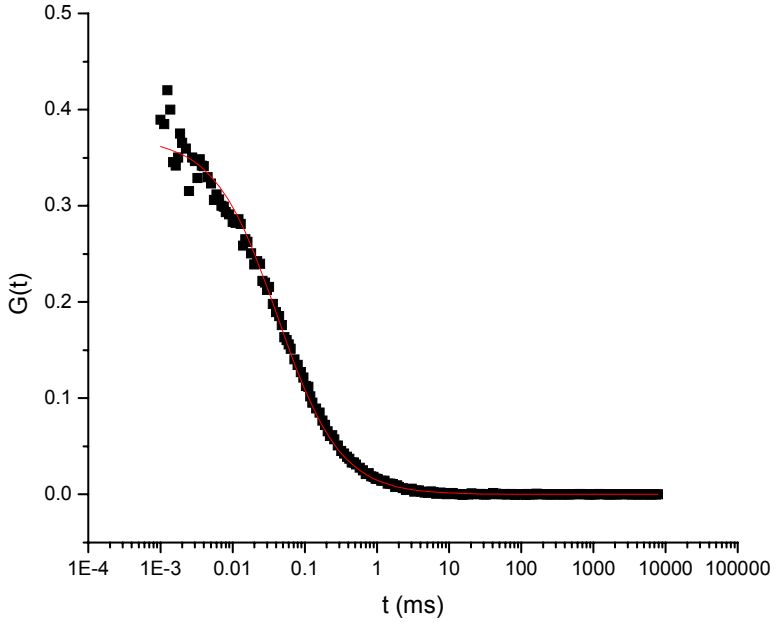

Figure 4-1. FCS set-up calibration. The autocorrelation curve obtained from a 10 nM rhodamine 123 aqueous solution was fitted with a mathematical model using a least-square fit algorithm. The values for the calculated radii were 0.22 μm for ω_{xy} and 1.56 μm for ω_z.

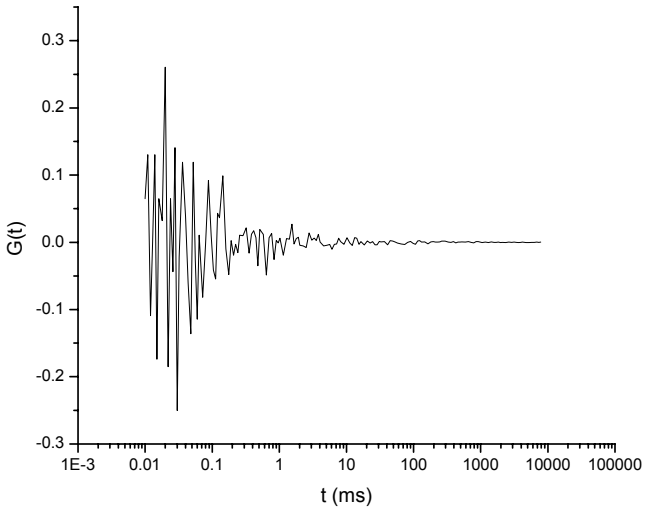

Figure 4-2. Autocorrelation function measured on the cell membrane of the BNL 1ME A.7R.1 and BNL CL.2 cell lines.

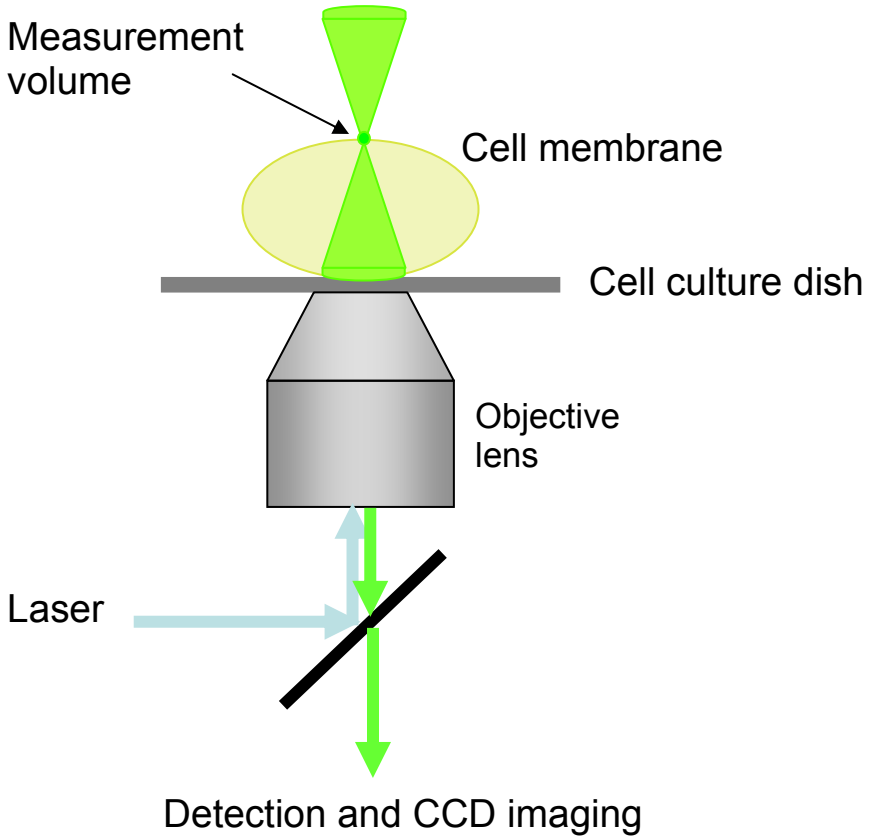

Figure 4-3. Aptamer-cell binding studies. The light coming from an Ar^+ laser excites a small volume element on the cell membrane. The laser beam focusing on the membrane is accomplished with the help of a CCD camera. The fluorescent light coming from the sample is then focused onto the detection optics.

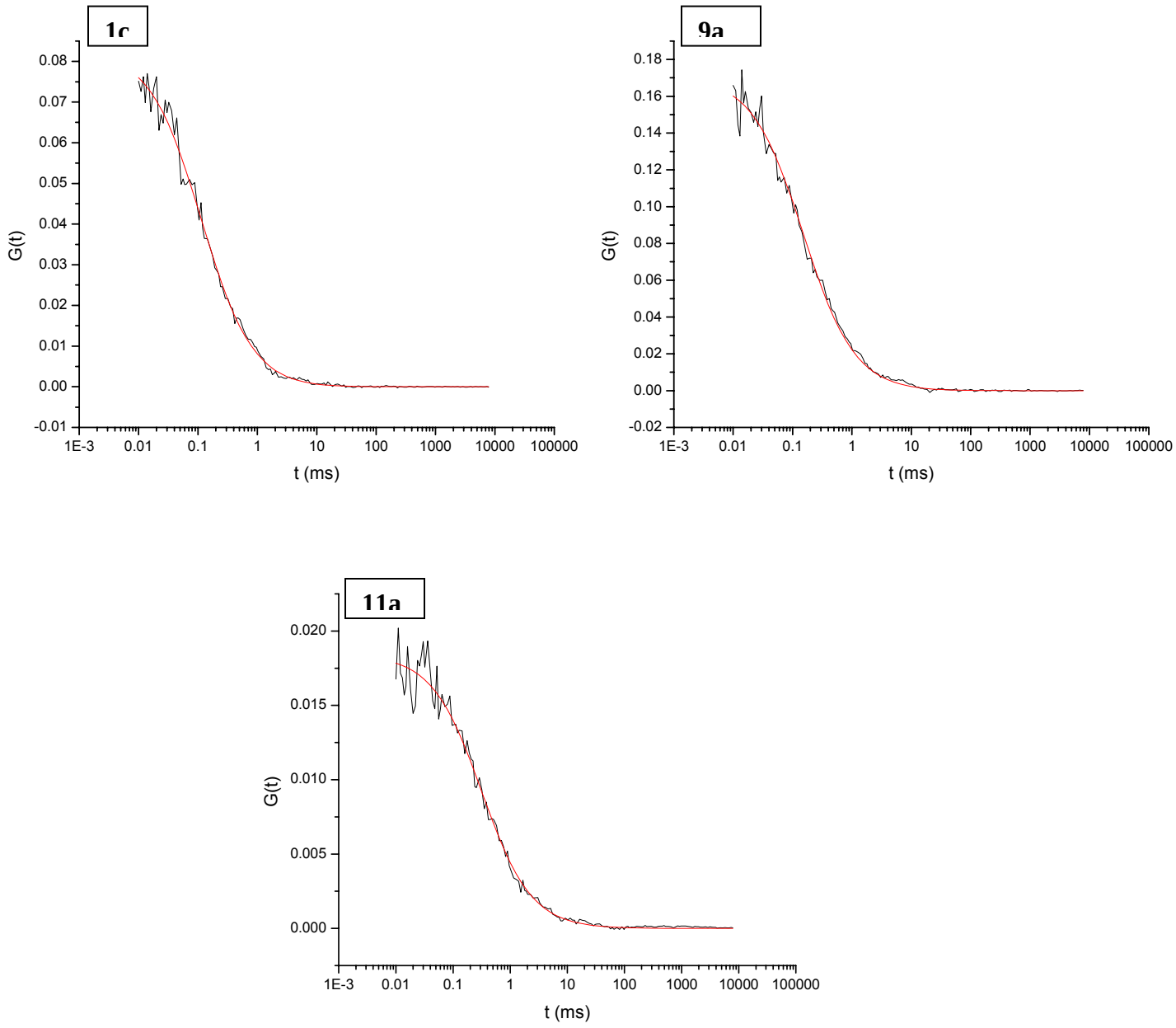

Figure 4-4. Autocorrelation curves for the FITC-labeled TLS aptamers. Diffusion times of 0.1 ms, 0.2 ms, and 0.3 ms were obtained for the fluorescently-labeled aptamers TLS 1c, TLS 9a, and TLS 11a, respectively.

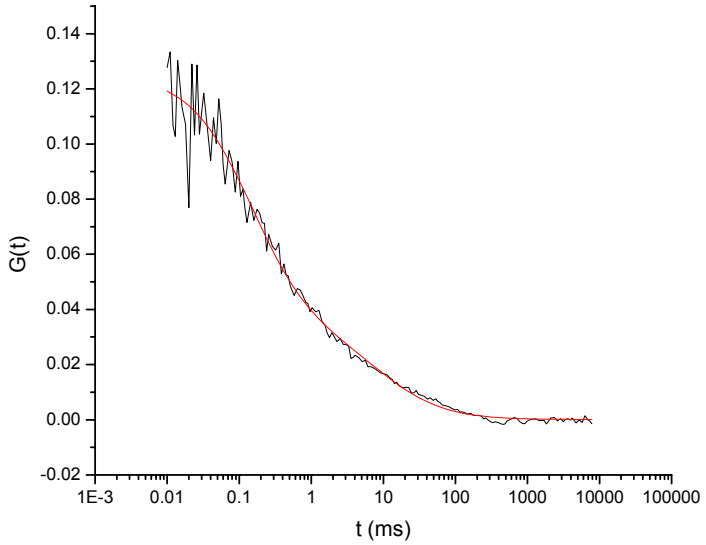

Figure 4-5. Autocorrelation curve for the IMEA cells after incubation with 3 nM FITC-labeled aptamer TLS9a. The diffusion times (τ_D) and corresponding fractions (y) were $\tau_D{}^{b}$ = 10.8 ms, y^b = 24% for the bound fraction, and $\tau_D{}^{f}$ = 0.2 ms, y^f = 76% for the free fraction.

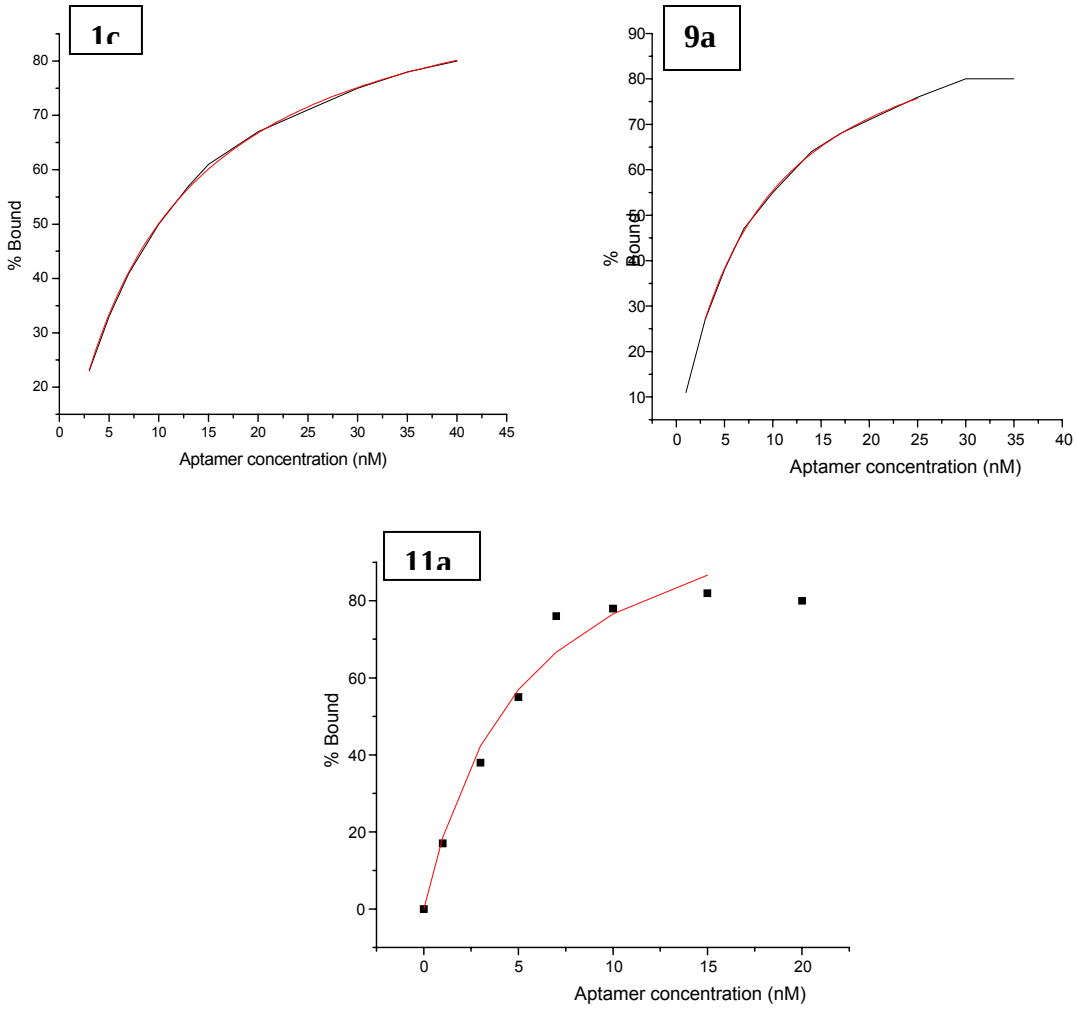

Figure 4-6. Binding curves for the TLS aptamers. Based on the half saturation, the K_D values were estimated to be ~10 nM for TLS 1c, ~ 8 nM for TLS 9a, and ~5.3 nM for TLS 11a, respectively.

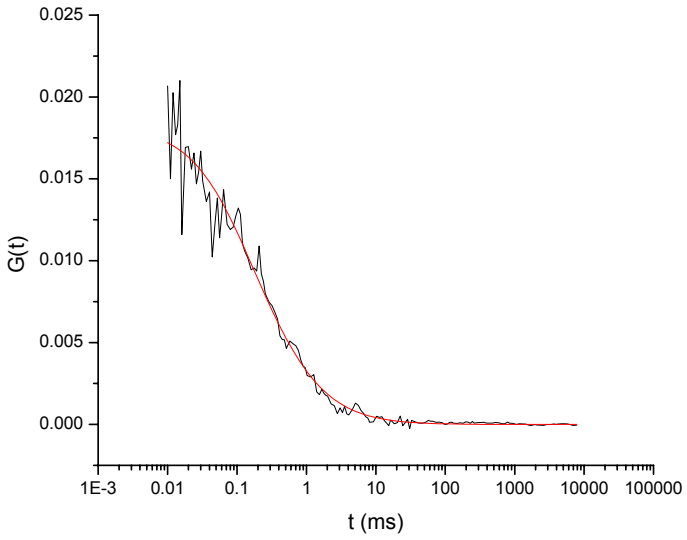

Figure 4-7. Autocorrelation curve for the displacement of membrane-bound labeled TLS 9a by postincubation of the cells with a thousand-fold molar excess of non-labeled aptamer. The fluorescently labeled aptamer bound to the cell membrane was almost completely replaced by the non-labeled aptamer after 3 hours of incubation.

CHAPTER 5
APTAMER BINDING TO CANCER CELLS: ESTIMATION OF RECEPTOR DENSITY ON THE CELL MEMBRANE

5.1 Introduction

Cell surface receptors, because they are restricted to the plasma membrane, are clustered in space. If diffusion can limit the rate of ligand-receptor interaction, theory predicts clustering to have the effect of reducing both the forward and reverse rate constants for ligand-receptor binding. The forward rate constant is reduced because nearby receptors compete for the same ligand and depress its concentration locally. The reverse rate constant is reduced because a ligand that dissociates from one receptor has a finite probability of binding to another before escaping from the vicinity of the cell. This effect of receptor density on ligand binding may have important consequences in biological systems since the rate at which ligands bind to cell surface receptors might serve to regulate the transmission of a chemical signal across the plasma membrane.

5.2 Materials and Methods

Cell lines. BNL 1ME A.7R.1 (mouse hepatoma) and HeLa (cervix adenocarcinoma) cell lines were obtained from American Type Culture Collection. The cells were cultured in Dulbecco's modified Eagle's medium (American Type Culture Collection), for mouse liver cancer cells, and in RPMI 1640 medium (American Type Culture Collection), for HeLa cells, with 10% fetal bovine serum (Invitrogen, Carlesbad, CA) and 0.5 mg/ml Penicillin-Streptomycin (American Type Culture Collection, Manassas, VA) at 37^{o}C under a 5% CO_2 atmosphere. The cells were grown in 8-well Nunc chambers (Nalge Nunc Inc., IL, USA) to a density of ~ 1000 cells/well. The cells were washed before and after aptamer incubation with Dulbecco's phosphate buffer (Sigma) with 5 mM $MgCl_2$. The aptamer solutions were prepared in the same buffer.

Aptamers. The aptamers used were TLS1c (5'- ACA GGA GTG ATG GTT GTT ATC TGG CCT CAG AGG TTC TCG GGT GTG GTC ACT CCT G-3'), TLS9a (5'- AGT CCA TTT TAT TCC TGA ATA TTT GTT AAC CTC ATG GAC-3'), TLS11a (5'- ACA GCA TCC CCA TGT GAA CAA TCG CAT TGT GAT TGT TAC GGT TTC CGC CTC ATG GAC GTG CTG-3'), and sgc8 (Figure 5.1). All the aptamers were selected, synthesized and HPLC-purified in our lab. They were used both in a non-labeled form and labeled with fluorescein isothiocyanate (FITC).

FCS instrumentation. FCS measurements were performed on a custom apparatus, which has been developed from an Olympus IX70, as described in Chapter 3. Briefly, the excitation light of a 488 nm line of an Ar-ion laser is focused onto the sample through a Olympus 60x numerical aperture 1.2 objective for water immersion. The fluorescence is collected by the same objective, separated from the excitation light by a dichroic mirror, then split by a 50/50 cube splitter and sent onto an avalanche photodiode (SPCM-AQR-14, Perkin Elmer) by the means of a 50 μm-inner diameter optical fiber after passing through a 515–555 nm bandpass filter. The sample is illuminated with an excitation power of 20 μW at the back aperture of the objective. The measurements are performed in a volume element of 0.4 fL with half-axes ω_{xy} = 0.22 μm and ω_z = 1.56 μm. Autocorrelation is processed by a hardware correlator (ALV 5000/EPP, ALV-GmBH, Langen, Germany). Data fitting was performed with MicroCal Origin using a least-square fit algorithm.

FCS data evaluation. The observed fluorescence intensity fluctuations occurring in the volume element are correlated and non-linear least square minimization is used to calculate the parameters of the intensity autocorrelation function $G(\tau)$.

When the volume element is projected onto the cell surface, both the bound FITC-labeled aptamer diffusing at the cell surface and the unbound FITC-labeled aptamer diffusing above the cell surface will be seen. The autocorrelation function for 3D diffusion of the unbound fluorescently labeled aptamer in solution above the cell surface and 2D diffusion of the bound labeled aptamer to membranes on the cell surface is given by:

$$G(\tau) = 1 + \frac{1}{N}\left[(1 - \sum y_i)\left(\frac{1}{1 + \tau/\tau_D{}^F}\right)\left(\frac{1}{1 + w^2\tau/\tau_D{}^F}\right)^{1/2} + \sum y_i \left(\frac{1}{1 + \tau/\tau_D{}^{Bi}}\right)\right] \quad (5\text{-}1)$$

where N is the number of molecules, $\tau_D{}^F = \omega_{xy}{}^2/4D_F$ for the unbound labeled aptamer, $\tau_D{}^B = \omega_{xy}{}^2/4D_B$ is the diffusion time for the bound labeled aptamer, $\sum y$ is the fraction of the bound aptamer diffusing with $\tau_D{}^B$, and $\sum (1 - y)$ is the fraction of the unbound aptamer diffusing with $\tau_D{}^F$.

The bi-molecular interactions between aptamers and cells are represented as:

$$A^* + R \overset{K_D}{\rightleftharpoons} A^*R$$

where A* is the fluorescently-labeled aptamer, and R is the cell receptor. The K_D values have been previously determined, as described in Chapter 4. The system can be characterized by the following equations:

$$K_D = \frac{[A^*] \text{ x } [R]}{[A^*R]}$$

$$[A^*]_{tot} = [A^*]_{free} + [A^*R]$$

$$[R]_{tot} = [R]_{free} + [A^*R]$$

$$y = \frac{y_{A^*R}}{y_{A^*free} + y_{A^*R}} = \frac{[A^*R]}{[A^*]_{tot}}$$

where $[A^*]_{tot}$ and $[R]_{tot}$ are the total concentrations of the labeled aptamer and receptors, respectively. The number of receptors can then be expressed from the equations as

$$[R]_{tot} = K_D \frac{y}{1 - y} + y \times [A^*]_{tot} \quad (5\text{-}2)$$

The receptor density on the cell membrane can then be estimated as follows:

$$r = ([R]_{tot} \times V \times N_A) / 2 \times (\text{cell membrane surface area}) \quad (5\text{-}3)$$

where V is the size of the volume element, N_A is Avogadro's number, and the cell membrane surface area can be estimated from the radius of the measurement volume in the radial direction, ω_{xy} (area = $\pi\ \omega_{xy}^2$).

5.3 Results and Discussion

The BNL 1ME A.7R.1 cells were incubated with 36 nM labeled TLS aptamers for 40 minutes at 4°C. Figure 5-2 shows the fitted autocorrelation curve obtained after incubation of the aptamer TLS 1c with the cells.

The K_D values were determined as described in Chapter 4. FCS measurements performed after incubation of cells with a saturating concentration of labeled aptamer provided the value for the bound fraction of the aptamer, *y*.

The total concentration of the receptor in the measurement volume for the TLS 1c aptamer was found to be 56.4 nM, which means ~6.8 receptors within the volume element. This allowed us to estimate the receptor density as being 44.4 receptors/μm^2.

For the TLS 9a aptamer we found a total receptor concentration of 58.4 nM, meaning about 7 receptors within the measurement volume or 46.2 receptors/μm^2.

Since the receptors responsible for binding the aptamers selected for liver cancer cells have not yet been determined, a comparison between their density on the cell membrane and that of an already established type of receptor was needed.

The chosen receptors were protein tyrosine kinase-7 (PTK7), which are receptor protein tyrosine kinase-like molecules that contain a catalytically inactive tyrosine kinase domain. This

class of receptors is expressed on the surface of HeLa cells and is recognized by the sgc8 aptamers, which were selected in our lab. The dissociation rate constant, as determined by flow cytometry, was 0.8 nM.

First, FCS was employed to determine the dissociation rate constant for the sgc8 aptamer binding to HeLa cells and its value was compared to the one previously calculated. Autocorrelation curves for the free and bound aptamers are shown in Figure 5-3. From Figure 5.3 (C), it can be seen that 1.3 nM labeled aptamer saturates the cell membrane receptors.

The binding curve of the sgc8 aptamer to PTK7 receptors on the surface of HeLa cells is shown in Figure 5.4. The K_D value, based on the half saturation concentration, was estimated to be ~0.72 nM.

Based on these results, the total receptor concentration for the sgc8 aptamer was found to be 7 nM, this meaning 1.9 receptors within the volume element. This allowed us to estimate the receptor density as being ~17.2 receptors/μm^2.

Since the PTK7 receptors on the surface of HeLa cells become saturated at much lower concentrations than the receptors for TLS aptamers on the surface of mouse liver cells, a lower density of the former receptors was to be expected.

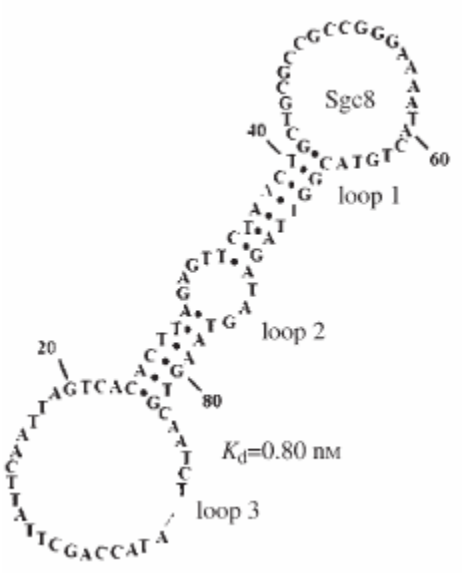

Figure 5-1. Structure of the sgc8 aptamer.

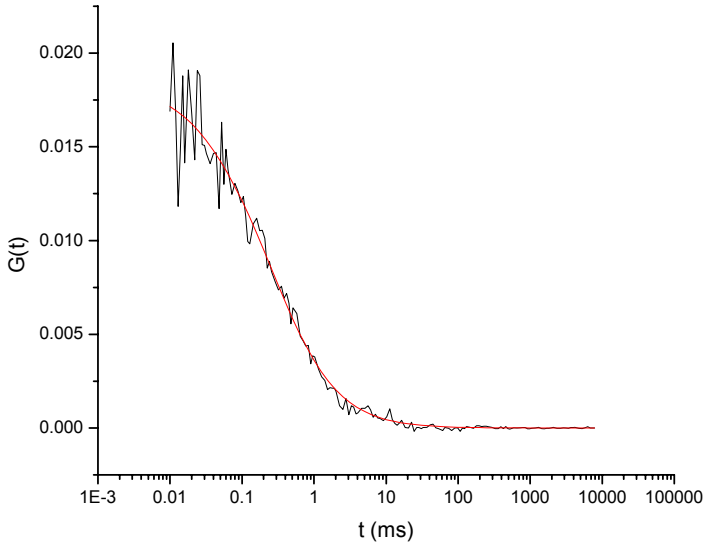

Figure 5-2. Autocorrelation curve for the BNL 1ME A.7R.1 cells after incubation with 36 nM FITC-labeled aptamer TLS1c. The diffusion times (τ_D) and corresponding fractions (y) were $\tau_D^{\,b}$ = 7.8 ms, y^b = 75% for the bound fraction, and $\tau_D^{\,f}$ = 0.1 ms, y^f = 25% for the free fraction.

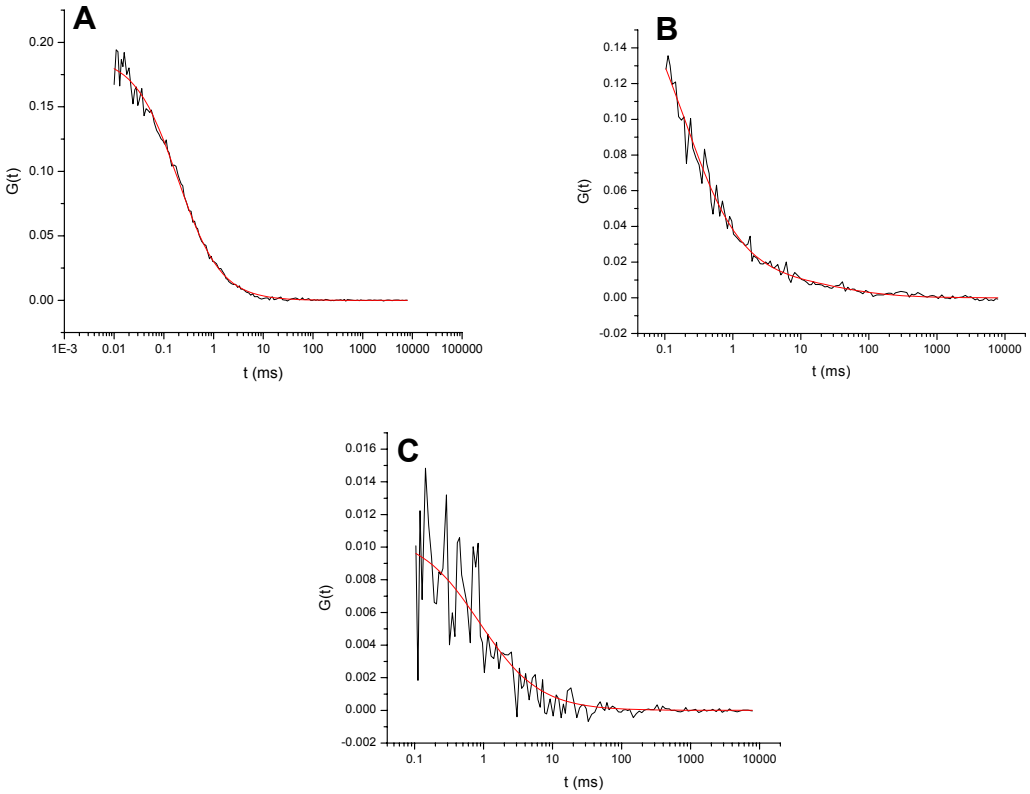

Figure 5-3. Autocorrelation curves for (A) free aptamer, diffusing with τ_D = 0.2 ms. (B) HeLa cells incubated with 0.1 nM aptamer; τ_D^{b} = 44.1 ms, y^{b} = 4.8% for the bound fraction, and τ_D^{f} = 0.2 ms, y^{f} = 95.2% for the free fraction. (C) HeLa cells incubated with 1.3 nM aptamer; τ_D^{b} = 44.1 ms, y^{b} = 88.9% for the bound fraction, and τ_D^{f} = 0.2 ms, y^{f} = 11.1% for the free fraction.

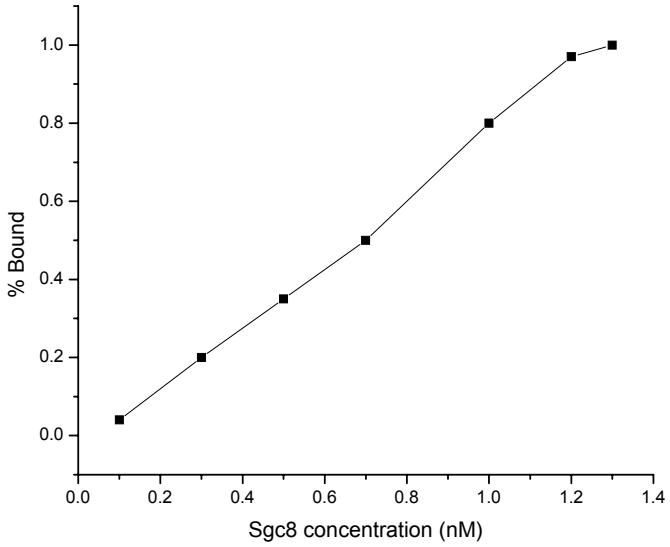

Figure 5-4. Binding curve for the sgc8 aptamer. Fractional saturation of the membrane bound labeled aptamer was obtained as a function of the ligand concentration in the binding medium. HeLa cells were incubated with buffer containing different concentrations of labeled aptamer for 40 min. at 4°C.

CHAPTER 6
SUMMARY, CONCLUSIONS AND FUTURE DIRECTIONS

6.1 Summary and Conclusions

It has already been established that FCS is the technique of choice for studying diffusion and reactions at the single molecule level. In the studies presented here it has been shown that the FCS setup built in our lab was capable of providing excellent sensitivity and enabled the study and determination of mass, diffusion coefficients, and binding properties of a variety of species. In addition, it proved to be an excellent tool for investigations into the binding properties of aptamers interacting with the cell membranes of live cancer cells.

To further understand the complexities of the cell based studies, several lines of discussion and understanding will now be explored since the totality of the cell based experiments have been discussed. For instance, in the study of a ligand-receptor interaction when the ligand is labeled with a fluorescent dye, it is of great importance to take into account the background fluorescence signal. Cell autofluorescence is a well known occurrence in which the naturally fluorescent proteins and molecules inside in the cell can be detected along with any fluorescent moieties that are necessary for the experiment. As such autofluorescence from the cell when in extremes, can significantly impact an experiment, especially one where sensitivity is required. This is especially true for a technique like FCS that not only monitors the fluorescence intensities but also fluctuations in the intensity. If the autofluorescence background was too high, the correlation function could be greatly impacted since the molecules causing the autofluorescence, e.g. naturally fluorescent proteins, likely would move little inside the cells mimicking the behavior of the fluorescently labeled aptamer bound to a surface protein. This could significantly affect the results of the binding coefficient experiments making the aptamer appear to bind with higher affinity and it could affect the binding receptor density measurements by

making the aptamer target appear more highly expressed. To check the background signals, the autofluorescence on the cell membranes without the addition of fluorescent ligands was measured. No significant background signal was detected on the surface membranes of mouse liver cancer cells or the HeLa cells. This indicates that the measured aptamer properties and receptor density measurements are not influenced by the autofluorescence of the cells in these cell lines. However, this is an important control that must be performed for each cell line utilized with FCS as different cell lines are likely to differ in their autofluorescence levels.

In the cell experiments, it is also important to understand the different possible populations of the aptamer in the system. This is due to the measurement volume of the FCS setup encompassing a greater thickness than the cell membrane itself. Since the focal volume was greater than the cell membrane, the unbound aptamer and bound aptamer would likely be measured in the cell experiments. Indeed, upon the incubation of cells with fluorescently labeled aptamers, the correlation analysis of the intensity fluctuations showed both the fraction of the aptamers bound to the cell membranes and the fraction of the unbound aptamers, due to the fact that the volume element extends into the space above the cell membrane. This leads to one of the advantages of using FCS for this type of determination as based on the correlation function of the measurement the bound and unbound probe in the system can be differentiated. This also serves as its own control for the FCS setup in that the diffusion coefficient for the unbound aptamer should remain constant throughout the experiments while the bound fraction on the cell membrane surface will vary depending on the parameters of the experiments.

In regards to varying the parameters of the experiments, changing the amount of the fluorophore-labeled aptamer in the system also affects the FCS measurements. As the amount of the bound aptamer changes in proportion to the amount of available cell membrane receptors, the

ratio of the bound to unbound aptamer also changes in accordance to the binding characteristics of the aptamer. Increasing concentrations of labeled aptamer in the buffer medium leads to an increased proportion of membrane-bound fraction. The aptamer binding curve was plotted as fractional saturation of the membrane-bound labeled aptamer vs. aptamer concentration in the binding medium. From this plot of the relationship between the aptamer and surface membrane receptor a great deal of information can be determined. One important parameter is the dissociation rate constant of the aptamer from the receptor. The dissociation rate constant was estimated to be the saturation at 50% binding.

In the course of the cellular experiments, it was also important to conduct some general control experiments to further confirm the veracity of the calculated results. To verify that the aptamer was binding specifically to its targeted receptor, the competitive displacement with non-labeled aptamer was examined. In this experiment a large excess of non-labeled aptamer competes against the labeled aptamer in binding to the targeted receptor. Since there are a limited number of receptors on the surface, the majority should be bound by the non-labeled aptamer given the huge excess of the nonlabeled population. If the labeled aptamers are not displaced by the unlabeled aptamers then there is no competition between them and the aptamers must not be interacting with their target receptor. Therefore, cells were incubated with labeled aptamer, and after 40 min a 1000-fold molar excess of non-labeled aptamer was added. This resulted in a reduction of the labeled aptamer binding, and after three hours the aptamer binding was almost entirely displaced. This indicates that the labeled aptamer was bound to the targeted receptor indicating that the aptamer was binding selectivity to that receptor. This serves to further validate the previously mentioned results as the aptamer must have been binding to its target and not simply undergoing a non-specific interaction with the cell membrane surface.

Further, a method for calculation of receptor density on cell membranes was proposed and applied for the estimation of the number of receptors per unit area of the molecules responsible for binding the TLS aptamers on the surface of mouse liver cancer cells and of PTK7 proteins expressed on the surface of HeLa cells. The density of PTK7 was found to be much smaller than that of the receptors binding the TLS aptamers, which is in accordance with the much lower value of the saturation concentration at half binding.

6.2 Future Directions

To confirm the accuracy of the proposed method for calculation of receptor density on cell membranes, more experiments need to be done. One important experiment involves the controlled decrease in the number of receptors available for binding the labeled aptamers. By incubating the cells with increasing concentrations of non-labeled aptamer and keeping the amount of labeled aptamer constant, we should observe a linear decrease in the calculated numbers of receptor densities.

Another way to confirm the reliability of the method is to calculate the density of the receptors for an already studied system, such as the expression of the receptors for IgE on the surface of RBL-2H3 cell line.[80]

APPENDIX
DEVELOPMENT OF A SUBMICROMETER-SIZE SOL – GEL-BASED NITRIC OXIDE SENSOR

A.1 Introduction

Nitric oxide (NO) is involved in important physiological processes, such as neurotransmission, immune function, hemostasis and vascular tone, as well as in pathophysiological conditions, including septic shock, atherosclerosis, ischemia/reperfusion injury, and carcinogenesis.[81,82]

In contrast to other cellular signal molecules, NO is synthesized and released without special storage and transfer mechanisms.[83-88] Its concentration in the cytosol of an endothelial cell, in the moment when it is being released, has been estimated to be ~1.3 μM.[87] Due to its very small size and hydrophobicity, its diffusion from a point source can affect targets a relatively long distance away from its origin (150-300 μm for a time of 4-15 seconds).[89-92]

A few examples of reactions in which NO has been observed to be involved are[81]: interaction with cytochrome P450 enzyme, which leads to the inhibition of this protein in mammalian cells; reaction with oxyhemoglobin or oxymioglobin, which is important for abating peroxide toxicity; reaction with superoxide, which is a detoxication mechanism for reactive oxygen species.

Given the multiple physiological and pathological effects of nitric oxide in many cell functions, the intracellular NO levels are considered potential variables affecting signal-transduction pathways.[93]

Due to its high reactivity, most of the methods currently available for detecting the *in situ* production of NO in cells are indirect.[94] For example, *in situ* hybridization allows an analysis of transcriptional changes in nitric oxide synthase (NOS) mRNAs. Immunocytochemistry allows the determination of the cellular and sub-cellular localization of each of the NOS sub-types

(neuronal, endothelial, and inducible) at the protein level. In addition, the NADPH-diaphorase histochemical reaction has been used as a potential marker of NO-synthesizing enzymes.[95,96]

Direct methods are available to measure NO or NO derivatives, such as nitrites and nitrates, released in cell media. These methods include chemiluminescence[97,98], the Griess spectrophotometric method[99,100], spin trapping using electron paramagnetic (EPR) resonance spectrometry,[101,102] electrochemistry,[103,104] and fluorescence[105-114]. However, the Griess method can only determine the concentration of nitrite which is the final metabolite of NO, the EPR technique does not have sufficient sensitivity,[114] the electrochemical methods respond to artifacts derived from other redox species, and the chemiluminescence detection requires the use of cytotoxic H_2O_2.[111]

Since it has been shown that the fluorescence methods are very reliable[105-108], and that they can provide both temporal and spatial data, researchers focused on developing new sensitive and selective fluorescent dyes.

Kojima et al. designed diaminofluoresceins (DAFs) as indicators for NO.[111] The fluorescent chemical transformation of DAFs is based on the reactivity of aromatic vicinal diamines with NO in the presence of dioxygen. The N-nitrozation of DAFs, yielding the highly green-fluorescent triazole form, offers the advantages of specificity, sensitivity, and a simple protocol for the direct detection of NO. 4-Amino-5-methylamino-2',7'-difluorescein (DAF-FM) has been reported to be the most photostable and sensitive member of this class of dyes.[112-114] With this indicator, the spectrum of the NO adduct is independent of pH above pH 5.5. A reported limit of detection with DAF-FM is 3 nm.[113] For the bioimaging of NO, DAF-FM diacetate has been synthesized, which permeates well into cells and is quickly transformed into DAF-FM by esterases in the cytosol. The reaction is depicted in Figure A-1.

Optical sensors. When designing an optical fiber-based chemical sensor, a molecule that is sensitive to the analyte to be detected is immobilized on one end of the fiber (the tip). The immobilization of this molecule can be done either by covalently linking it to the tip surface, or by entrapping or attaching it to a matrix that will be deposited on the fiber tip. The optical fiber will be then coupled to an instrumental set-up equipped with an excitation source and a detector. Two different interfaces will be thus formed at the fiber ends: a chemo-optical interface (the fiber tip) and an opto-electronic interface (at the fiber end coupled to the instrument).[115] The fiber tip will be put in contact with the sample containing the analyte, which will cause changes in the optical properties of the molecule that is attached to the fiber (e.g. absorbance, fluorescence, reflectance). Next, such changes are converted into analytical signal at the optoelectronic interface.

Optical sensors have some advantages over electrochemical sensors, such as the fact that they do not require a reference electrode and the optical signal is not influenced by electrical interferences.

Many optical sensors based on fluorescent dye entrapment inside gels have been designed. Sol-gels have, however, several advantages over organic polymer supports, including physical rigidity and high abrasion resistivity; negligible swelling in both aqueous and organic solutions; chemical inertness; high biodegradational, photochemical, and thermal stability; excellent optical transparency and low intrinsic fluorescence.[116]

Sol-gel chemistry. The most important synthesis variables controlling the final morphology and physical properties of the sol-gels are the catalyst (acid or base), pH, water-to-siloxane ratio, and temperature. The sol-gel reaction scheme is shown in Figure A-2.

An acid catalysis (pH < 2) is characterized by weakly branched microporous structures, with particles growing up to ~ 4 nm and significantly higher porosity and dimensional shrinkage than the base catalyzed sol-gels.[117-124] Successful thin layer glasses were formed when an acid catalyst was used.[125]

The water-to-alkoxide ratio is very important for the final properties of the sol-gel. It was found that the sol-gel solutions were coatable when the water content was in the range of 40 to 70 mol%.[125] Since the alkoxide is immiscible with water, an alcohol is used as a solvent. Also, it has been observed that increasing the temperature (up to 70ºC) resulted in an overall decrease in condensation time.[126,127]

In this work, the sensitivity and selectivity of DAF-FM dye was used in conjunction with the reliability provided by an optical fiber-based detection set-up to develop a NO optical sensor.

A.2 Experimental Design and Methods

Materials. Tetramethyl orthosilicate (TMOS), dimethyldimethoxysilane (DMSMS) (Aldrich), methyltrimethoxysilane (MTMS), cetyltrimethylammonium bromide (CTAB), N-2-hydroxyethylpiperazine-N'-2-ethanesulfonic acid (HEPES) (Sigma Chemicals, Co.), methanol, HCl, H_2SO_4, NaCl, KCl, $CaCl_2$, $MgCl_2$, $NaHCO_3$, Na_2HPO_4, KH_2PO_4, dimethyl sulfoxide (DMSO) (Fisher Scientific), and 4-amino-5-methylamino-2',7'-difluorescein (DAF-FM) (Molecular Probes) were used for the sol-gel matrix preparation. (±)-(E)-2-[(E)-Hydroxyimino]-6-methoxy-4-methyl-5-nitro-3-hexenamide (NOR-1) (Sigma Chemicals, Co) was used as a nitric oxice donor. Distilled, deionized water (Easy Pure LF, Barnstead Co.) was used for the preparation of various aqueous solutions.

The optical fibers were obtained from Fiberguide Industries, Inc.

Instrumentation. The fluorescence measurements on the bulk doped sol-gel were performed using a SPEX Industries spectrofluorometer, model F-112A, and data was collected using DataMax software (Edison, New Jersey).

The fiber optic-based measurements were performed using an instrumental set-up like the one depicted in Figure A-3. Briefly, the light coming from an Ar^+ laser was focused onto a multimode optical fiber by the means of an objective lens. The probe was immobilized onto the opposite end of the fiber, which was immersed into the analyte solution. The fluorescence coming from the sample was transmitted back through the fiber and detected by a photomultiplier tube.

An XSafire microplate reader (TECAN Austria Ges. M.b.h.) was used for absorption measurements.

NO release. An organic NO donor, NOR-1, was used as a nitric oxide source. The reaction of NOR-1 leading to NO release can be depicted as follows:[128]

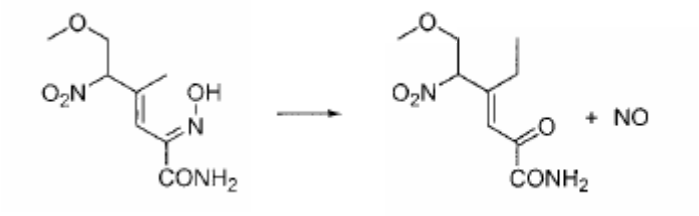

(A-1)

The DAF-FM reaction with NO is proposed to involve nitrous anhydride (N_2O_3). N_2O_3 is generated according to the following scheme:[129]

$$2NO + O_2 \longrightarrow 2NO_2 \qquad \text{(A-2)}$$

$$2NO_2 + 2NO \rightleftharpoons 2N_2O_3 \qquad \text{(A-3)}$$

According to this reaction scheme, the formation of the N-nitrosation species, N_2O_3, requires two molecules of NO. Therefore, the stoichiometry of the reaction between DAF-FM

and NO is 1:2. This also means that DAF-FM does not react directly with NO, but it reacts with the oxidized form of NO. However, it has been observed that in the absence of NO in the medium, the fluorescent benzotriazole derivative of the dye would not form.[129]

Sol-gel synthesis. Different water-to-alkoxide ratios, pH values, and alkoxide precursors were tested to optimize the quality of the sol-gel, both in terms of mechanical resistance, ability to retain the dye molecules inside the pores, as well as optical transparency. To test the quality of the synthesized sol-gels, measurements were performed for both a thin layer gel, analyzed using the laser set-up, and for monolithic gels, analyzed using the spectrofluorometer. The results showed that a less brittle and transparent gel, providing a good entrapment of the dye inside the pores, was obtained with an acid catalyst (pH < 1), using TMOS as an alkoxide precursor, with water-to-alkoxide ratios of 4.

The gels were prepared using 0.1 M HCl as a catalyst, a water-to-siloxane ratio of 4, and TMOS as a siloxane. Gels with both 1 μM and 5 μM DAF-FM were prepared, and each of them was made in duplicate, one set with methanol added, and the other without methanol. In addition, for each type of gel prepared, condensation reactions were allowed to occur at room temperature or at 70ºC.

Coating of the optical fibers. Sol-gel coating of the fibers was performed by the dip coating technique, which is depicted in Figure A-4.

Optical fibers 5 μM in diameter were cut into about 5 cm-length pieces and at one end the cladding was removed over a length of 1 cm. The bare tips were then immersed in concentrated HCl solution for 30 minutes. Sol-gel mixtures were prepared and allowed to stay at room temperature for 24 hours, under magnetical stirring. After drying, the tips of the optical fibers

were immersed in sol-gel solutions, withdrawn after about 10 seconds, and then allowed to stay in a vertical position, with the tips down, in a light-protected, closed container for one week.

A.3 Results and Discussion

Solution experiments. DAF-FM response to different NO concentrations was assessed for a 1 μM DAF-FM solution in pH 7.4 phosphate buffer. Upon addition of different concentrations of NOR-1, the dye fluorescence was measured by the spectrofluorometer. Due to the irreversibility of the reaction between DAF-FM and NO, after measuring the signal for the dye in buffer, small aliquots of the NO-releasing donor were added to the solution. The increase of fluorescence intensity with increasing NO concentration is shown in Figure A-5. A linear dependence of the fluorescence intensity on the NO concentration has been observed.

Bulk gel experiments. The change in DAF-FM fluorescence with varying NO concentrations was measured for monolith dye-doped sol-gels. After each NOR-1 solution addition, the fluorescence signal was monitored until a constant intensity was reached, because we anticipated that the diffusion through the bulk gel pores should take some time.

The response obtained for the 1 μM dye-doped gel condensed at 70ºC in the presence of methanol is shown in Figure A-6a. In the Figure A-6b, the signal stabilization monitored after the first NOR-1 addition is shown. The response of the 1 μM dye-doped gel condensed at room temperature without the addition of methanol is shown in Figure A-7. From these figures it can be easily seen that the dye entrapped inside the gel condensed at 70ºC in the presence of methanol shows a higher fluorescence signal upon the addition of nitric oxide.

Dye leaching experiments. The leaching of the dye out of the gel pores was also analyzed. The same types of gels as previously described were prepared and each of them was immersed in pH 7.4 phosphate buffer solution. The fluorescence intensity of the buffer solution was then measured at certain times. At each time interval, a small aliquot of the buffer was taken

out and placed into a cuvette, and after the fluorescence intensity measurement, the solution was added back into the gel container. The leaching of the two types of 1 μM dye-doped gels is presented in Figure A-8. The graph shows that the leaching of the dye entrapped inside the gel condensed at 70ºC in the presence of methanol was more pronounced than the leaching of the dye encapsulated inside the gel condensed at room temperature without the addition of methanol.

Optical fiber experiments. The fluorescence transmitted through the fiber dip-coated with 1 μM dye-doped gel was assessed before and upon addition of 200 μM NOR-1-released NO. The images obtained for the 1 μM dye-doped gel condensed at 70ºC in the presence of methanol, before and after NO donor addition, are shown in Figure A-9. The average fluorescence intensity for the whole flat surface of the tip was 1366.49 units before donor addition and 1696.41 units after NOR-1 addition.

From this set of experiments it was apparent that the dye leaching was higher for gels condensed at 70ºC in the presence of methanol, but their response to NO was more pronounced, most probably because of an easier diffusion through the pores. Leaching was also observed in the fiber optic experiments. In addition, when deposited on the fibers, there was a visible gel cracking on the flat surface of the tip.

Many attempts have been made to create a robust thin film of sol-gel with pores small enough to contain the dye molecules, but a satisfactory system has not yet been created.

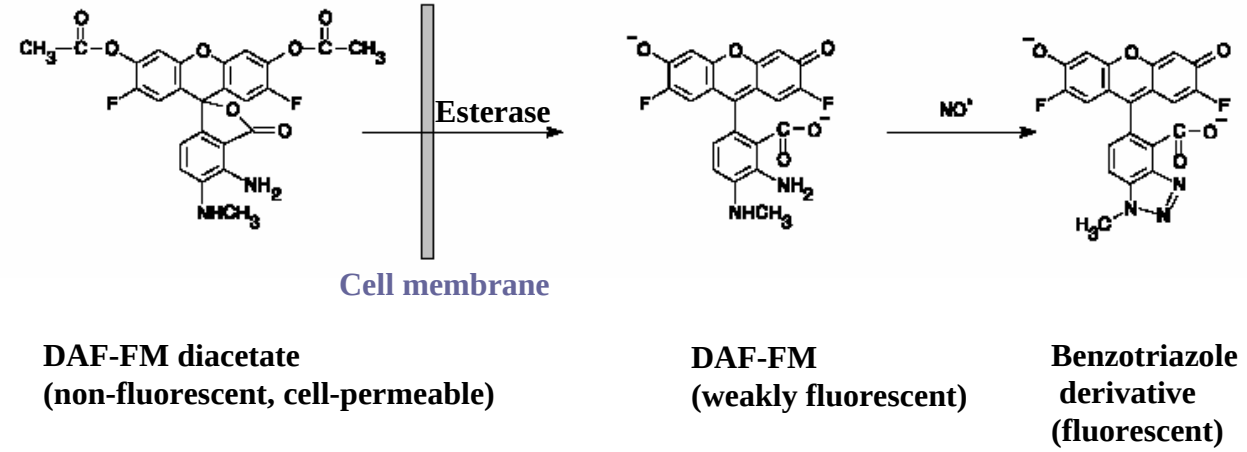

Figure A-1. Reaction scheme for the detection of NO by DAF-FM and DAF-FM diacetate.

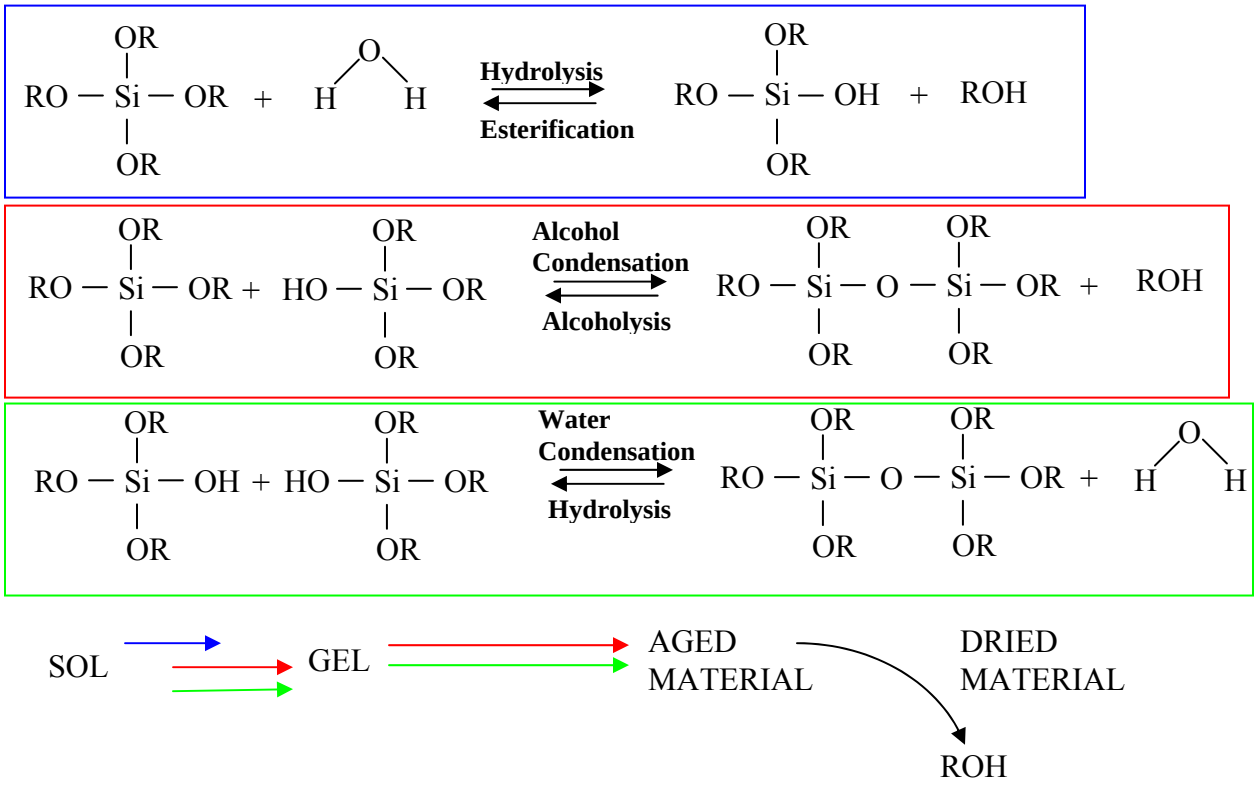

Figure A-2. Sol-gel reaction scheme. Hydrolysis and condensation reactions occur concurrently, but one reaction can be favored over the other depending on the reaction conditions. The condensation reactions continue long after the gel point and produce a strengthening, stiffening, and shrinkage of the network, which results in the spontaneous expulsion of solvent from the pores.

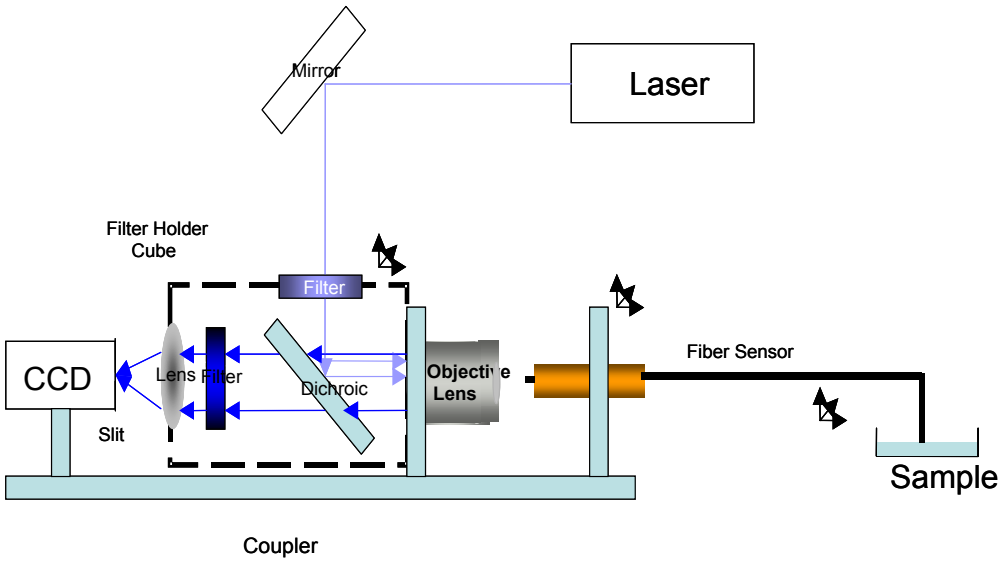

Figure A-3. Instrumental set-up. The light coming from an Ar^{+} laser is reflected by a dichroic mirror and focused onto a multimode optical fiber by the means of an objective lens. A DAF-FM-doped sol-gel layer is immobilized onto the opposite end of the fiber, which is immersed into a NO-containing solution. The fluorescence coming from the sample is transmitted back through the fiber, passed by the dichroic mirror, and after being filtered by an emission filter, is focused on a photomultiplier tube with the help of a lens.

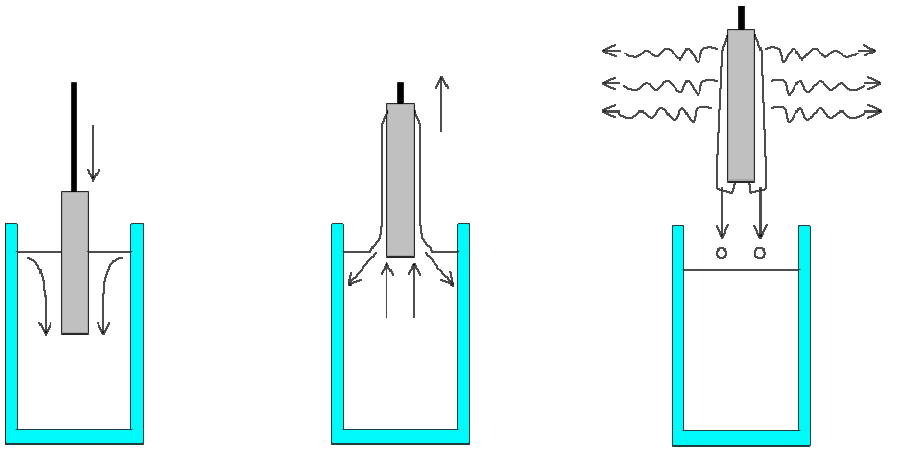

Figure A-4. Stages of the dip coating process: dipping of the substrate into the coating solution, wet layer formation by withdrawing the substrate and gelation of the layer by solvent evaporation

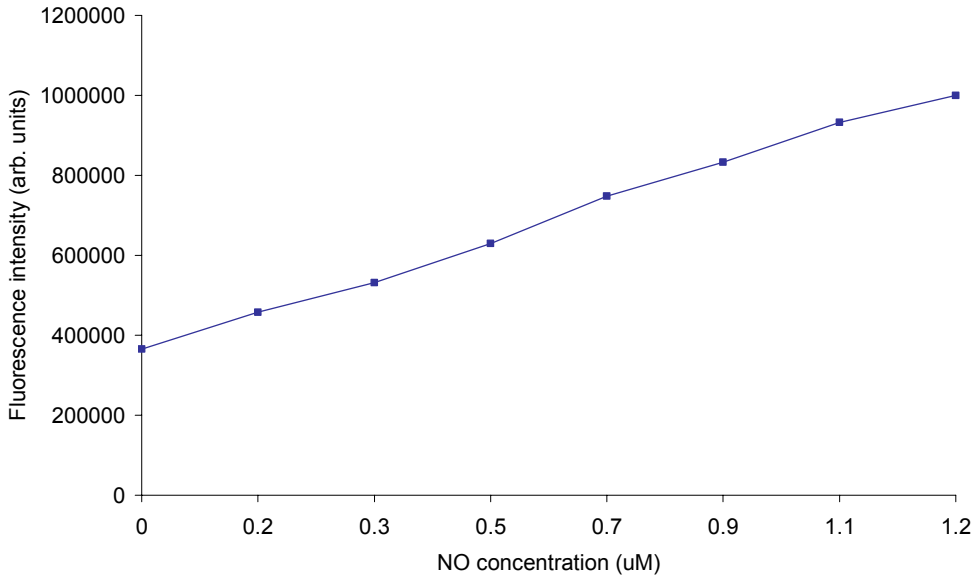

Figure A-5. Response of DAF-FM dye (1 μM) to different NO concentrations. There is a linear dependence of the fluorescence intensity on the NO concentration.

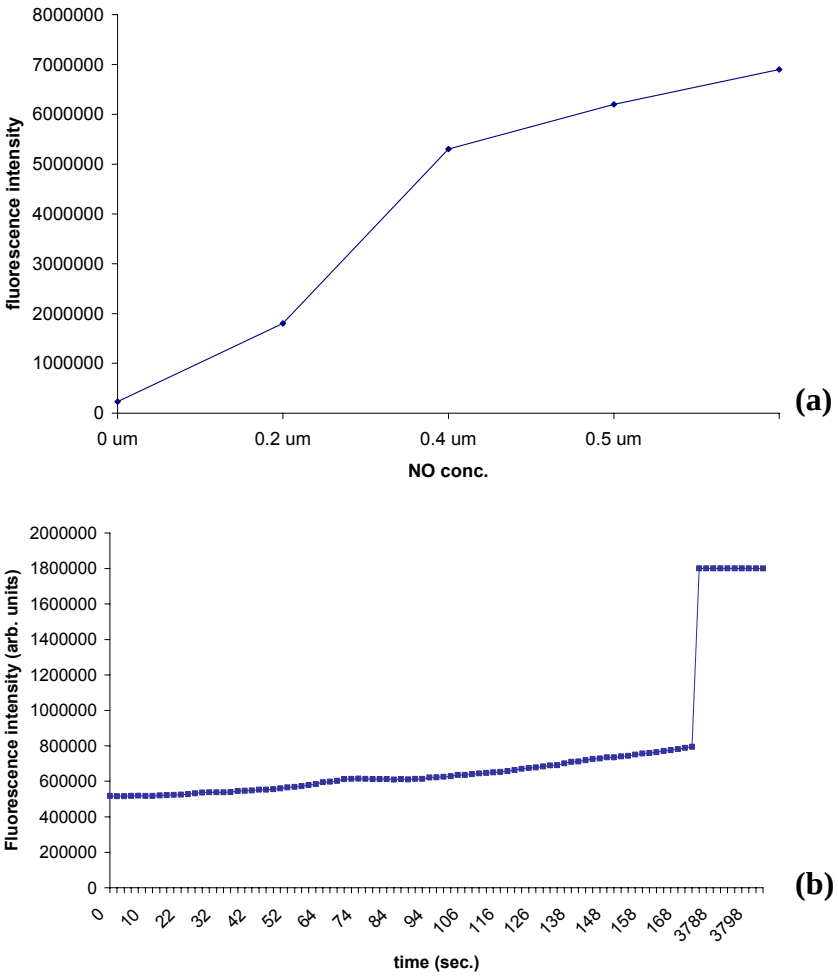

Figure A-6. (a) Response of the 1 μM dye-doped gel condensed at 70ºC in the presence of methanol to nitric oxide addition; (b) Signal stabilization after the first NOR-1 addition, for the same gel.

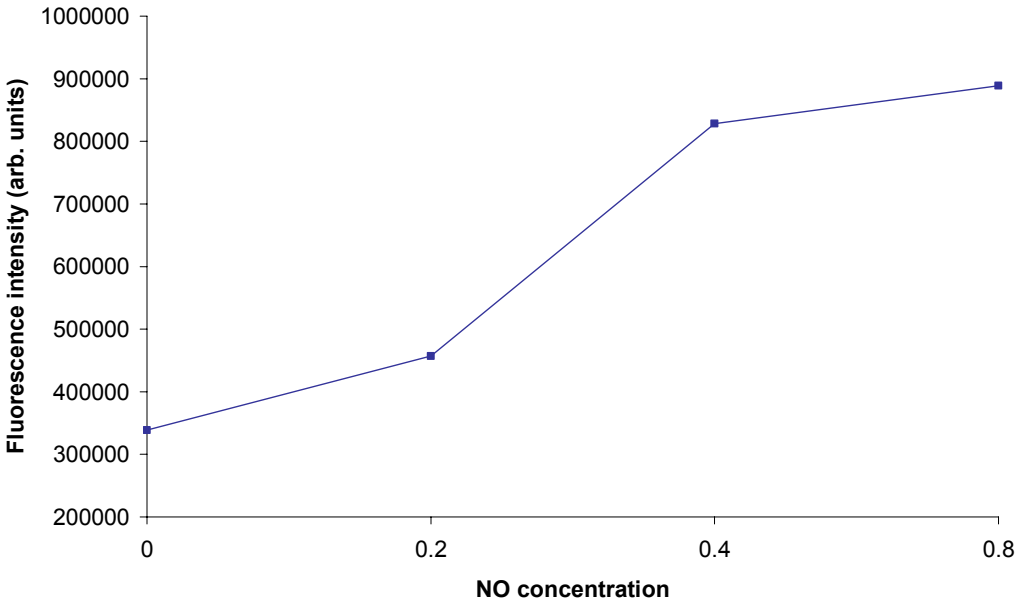

Figure A-7. Response of a 1 μM dye-doped gel condensed at room temperature without methanol addition, to nitric oxide addition.

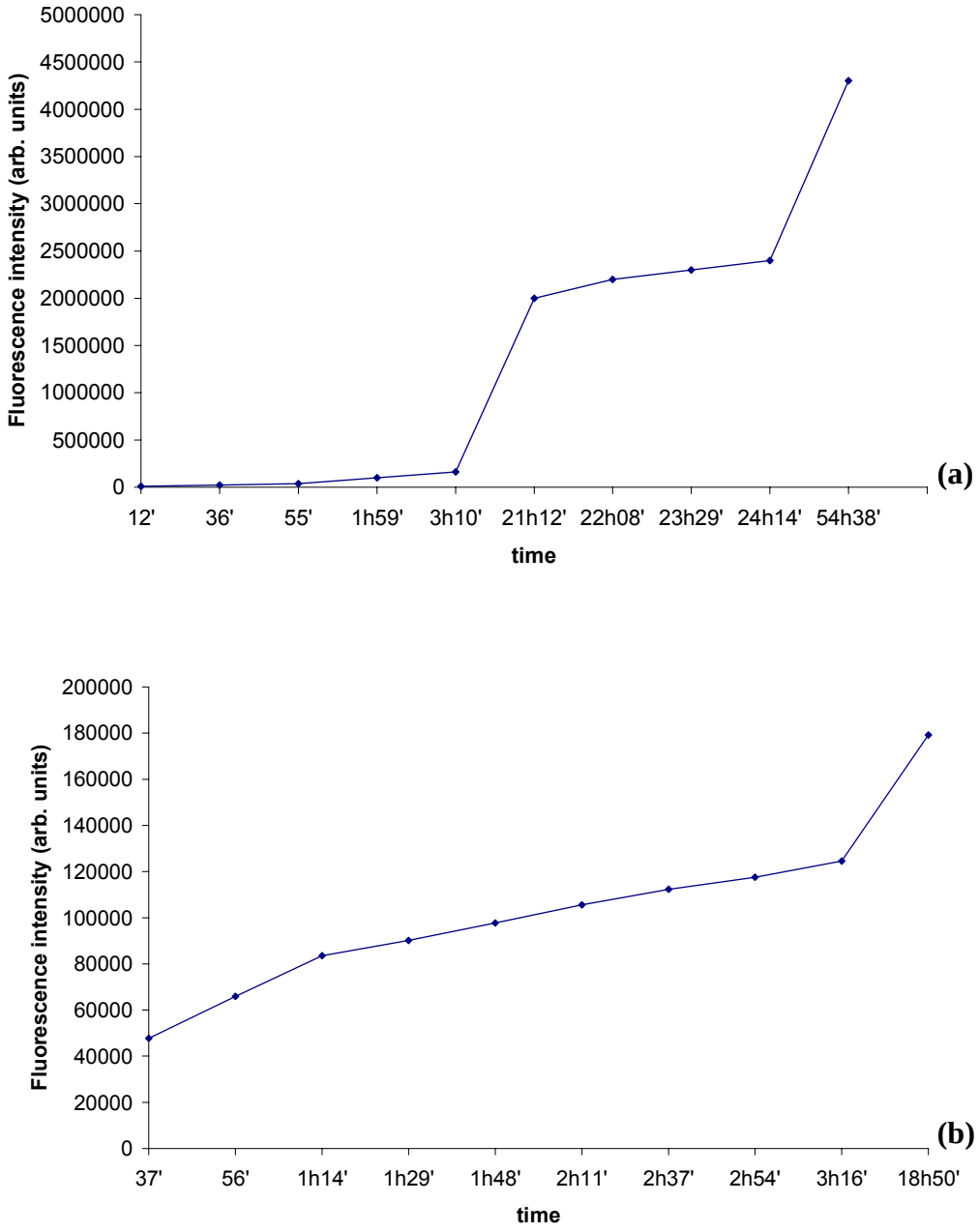

Figure A-8. (a) Leaching of the 1 μM dye-doped gel condensed at 70ºC in the presence of methanol; (b) Leaching of the 1 μM dye-doped gel condensed at room temperature without methanol addition.

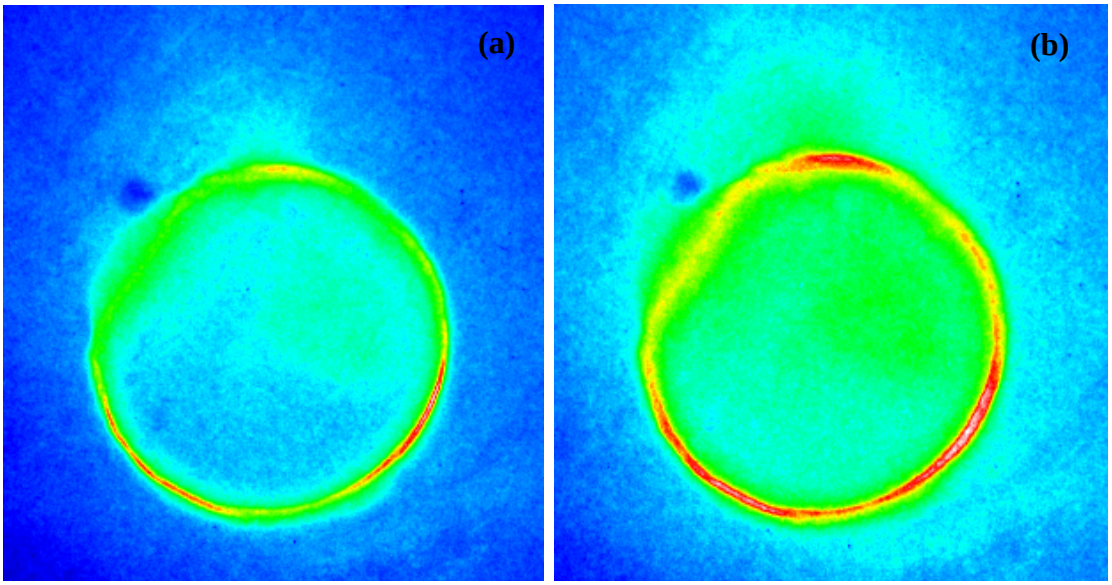

Figure A-9. CCD images of 5-μM optical fibers coated with 1 μM dye-doped gel condensed at 70ºC in the presence of methanol. (a) Before NO addition; (b) After 200 μM NO addition.

LIST OF REFERENCES

(1) Kruger, K., Grabowski, P. J., Zaug, A. J., Sands J., Gottschling D. E., Cech, T. R. *Cell* **1982**, *31*, 147–157.

(2) Stark, B. C.; Kole, R.,; Bowman, E. J.; Altman, S. *Proc. Natl Acad. Sci. USA* **1978**, *75*, 3712–3721.

(3) Robertson, D. L.; Joyce, G. F. *Nature Struct. Biol.* **1990**, *344*, 467–468.

(4) Tuerk, C.; Gold, L. *Science* **1990**, *249*, 505–510.

(5) Ellington, A. D.; Szostak, J. W. *Nature* **1990**, *346*, 818–822.

(6) Wilson, C.; Szostak, J. W. *Nature* **1995**, *374*, 766–767.

(7) Seelig, B.; Jaschke, A. *Chem. Biol.* **1999**, *6*, 167–176.

(8) Gilbert, W. *Nature* **1986**, *319*, 818-820.

(9) Cox, J. C., Hayhurst, A., Hesselberth, J., Bayer, T. S., Georgiou, G., Ellington A. D. *Nucleic Acids Res.* **2002**, *30*, e108.

(10) Cox, J. C.; Rudolph, P.; Ellington, A. D. *Biotechnol. Prog.* **1998**, *14*, 845–850.

(11) Ellington, A. D.; Cox, J. C.; Lee, J. F.; Collett, J. R. *The RNA World* 3rd edn: Cold Spring Harbor Press, New York, **2006**, 683–719.

(12) Shangguan, D.; Li, Y.; Tang, Z.; Cao, Z. C.; Chen, H. W.; Mallikaratchy, P.; Sefah, K.; Yang, C. J.; Tan, W. **2006**,*103*,11838-11843.

(13) Adam, G.; Delbruck, M. *Structural Chemistry and Molecular Biology*: W. H. Freeman, San Francisco, **1968,** 198–215.

(14) Berg, H. C.; Purcell, E. M. *Biophys. J.* **1977**, *20*, 193–219.

(15) DeLisi, C.; Wiegel, F. W. *Proc. Natl. Acad. Sci. USA.* **1981**, *78*, 5569 –5572.

(16) Shoup, D.; Szabo, A. *Biophys. J.* **1982**, *40*, 33–39.

(17) Berg, O.; von Hippel, P. H. *Annu. Rev. Biophys. Biophys. Chem.* **1985**, *14*, 131–160.

(18) Northrup, S. H.; Curvin, M. S.; Allison, S. A.; McCammon, J. A. *J. Chem. Phys.* **1986**, *84,* 2196 –2203.

(19) Northrup, S. H. *J. Phys. Chem.* **1988,** *92*, 5847–5850.

(20) Zwanzig, R. *Proc. Natl. Acad. Sci. USA.* **1990**, *87,* 5856 –5857.

(21) Wang, D.; Gou, S.; Axelrod, D. *Biophys. Chem.* **1992**, *43*, 117–137.

(22) Axelrod, D.; Wang, M. D. *Biophys. J.* **1994**, *66*, 588–600.

(23) Forsten, K. E.; Lauffenburger, D. A. *J. Comp. Biol.* **1994**, *1*,15–23.

(24) Lauffenburger, D. A.; Forsten, K. E.; Will, B.; Wiley, H. S. *Ann. Biomed. Eng.* **1995**, *23,* 208 –215.

(25) Goldstein, B.; Dembo, M. *Biophys. J.* **1995**, *68*, 1222–1230.

(26) Balgi, G.; Leckband, D. E.; Nitsche, J. M. *Biophys. J.* **1995**, *68*, 2251–2260.

(27) Model, M. A.; Omann, G. M. *Biophys. J.* **1995**, *69*, 1712–1720.

(28) Erickson, J.; Goldstein, B.; Holowka, D.; Baird, B. *Biophys. J.* **1987**, *52*, 657– 662.

(29) Goldstein, B.; Posner, R. G.; Torney, D. C.; Erickson, J.; Holowka, D.; Baird, B. *Biophys. J.* **1989**, *56*, 955–966.

(30) Erickson, J. W.; Posner, R. G.; Goldstein, B.; Holowka, D.; Baird, B. *Biochemistry* **1991**, *30*, 2357–2363.

(31) Pearce, K. H.; Hiskey, R. G.; Thompson, N. L. *Biochemistry* **1992**, *31*, 5983–5995.

(32) Duschl, C.; Sevin-Landais, A.; Vogel, H. *Biophys. J.* **1996**, *70*, 1985–1995.

(33) Lookene, A.; Chevreuil, O.; Østergaard, P.; Olivecrona, G. *Biochemistry* **1996,** *35*, 12155–12163.

(34) Otis, T. S.; Wu, Y.; Trussell, L. O. *J. Neurosci.* **1996**, *16*, 1634 –1644.

(35) Magde, D.; Elson, E.; Webb, W. W. *Phys. Rev. Lett.* **1972,** *29,* 705–708.

(36) Thompson, N. L. *Topics in Fluorescence Spectroscopy Techniques* vol. 1, ed. J. R. Lakowicz (New York: Plenum) **1991,** 337–378.

(37) Rigler, R; Mets, U; Widengren, J.; Kask, P. *Eur. J. Biophys.* **1993,** *22***,**169–175.

(38) Eigen, M.; Rigler, R. *Proc. Natl Acad. Sci. USA* **1994,** *91*, 5740–5747.

(39) Nie, S. M., Chiu, D.T., Zare, R.N., *Science* **1994**, *266*, 1018-1022.

(40) Krichevsky, O., Bonnet, G. *Rep. Prog. Phys.* **2002**, *65*, 251-297.

(41) Berland, K. M. *Biophys. J.* **1997,** *72*, 1487–1488.

(42) Gennerich, A.; Schild, D. *Biophys. J.* **2002**, *83*, 510–522.

(43) Amediek, A.; Haustein, E.; Scherfeld, D.; Schwille, P. *Single Mol.* **2002**, *3*, 201–210.

(44) Magde, D.; Elson, E.L.; Webb, W.W. *Phys. Rev. Lett.* **1972,** *29*, 705–708.

(45) Bacia, K.; Schwille P. *Methods* **2003**, *29*, 74–85.

(46) Elson, E.L.; Magde, D. *Biopolymers* **1974,** *13,* 1–27.

(47) Magde, D.; Elson, E.L.; Webb, W.W. *Biopolymers* **1974,** *13*, 29–61.

(48) Rigler, R.; Widengren, J. *Bioscience* **1990**, *3*, 180–183.

(49) Rigler, R.; Mets, U.; Widengren, J.; Kask, P. *Eur. Biophys. J.* **1993,** *22*, 169–175.

(50) Chen, Y.; Muller, J.D.; So, P.T.C.; Gratton, E. *Biophys. J.* **1999**, *77,* 553–567.

(51) Muller, J.D.; Chen, Y.; Gratton, E. *Biophys. J.* **2002,** *78*, 474–486.

(52) Chen, Y.; Muller, J.D.; Ruan, Q.Q.; Gratton, E. *Biophys. J.* **2002,** *82*, 133–144.

(53) Kask, P.; Palo, K.; Fay, N.; Brand, L.; Mets, U.; Ullmann, D.; Jungmann, J.; Pschorr, J.; Gall, K. *Biophys. J.* **2000,** *78*, 1703–1713.

(54) Thompson, N.L. *Topics in Fluorescence Spectroscopy*, Plenum, New York, **1991**, vol. 1, 337–378.

(55) Krichevsky, O.; Bonnet, G. *Rep. Prog. Phys.* **2002,** *65*, 251–297.

(56) Widengren, J.; Mets, U.; Rigler, R. J. *Phys. Chem*. **1995,** *99,* 13368–13379.

(57) Widengren, J.; Schwille, P. *J. Phys. Chem. A* **2000,** *104,* 6416–6428.

(58) Haupts, U.; Maiti, S.; Schwille, P.; Webb, W.W. *Proc. Natl. Acad. Sci. USA* **1998,** *95,* 13573–13578.

(59) Bacia, K.; Majoul, I.V.; Schwille, P. *Biophys J.* **2002,** *83,* 1184–1193.

(60) Dittrich, P.; Malvezzi-Campeggi, F.; Jahnz, M.; Schwille, P. *Biol. Chem.* **2001,** *382*, 491–494

(61) Meseth, U.; Wohland, T.; Rigler, R.; Vogel, H. *Biophys. J.* **1999,** *76,* 1619–1631.

(62) Kinjo, M.; Rigler, R. *Nucleic Acids Res.* **1995,** *23,* 1795–1799.

(63) Rauer, B.; Neumann, E.; Widengren, J.; Rigler, R. *Biophys. Chem*. **1996,** *58,* 3–12.

(64) Schwille, P.; Oehlenschlager, F.; Walter, N.G. *Biochemistry* **1996,** *35,* 10182–10193.

(65) Schuler, J.; Frank, J.; Trier, U.; Schafer-Korting, M.; Saenger, W.A. *Biochemistry* **1999,** *38*, 8402–8408.

(66) Brinkmeier, M.; Dorre, K.; Stephan, J.; Eigen, M. *Anal. Chem.* **1999,** *71*, 609–616.

(67) Brinkmeier, M. *Fluorescence Correlation Spectroscopy: Theory and Applications*: Springer, Berlin, **2001**, 379–395.

(68) Weidemann, T.; Wachsmuth, M.; Tewes, M.; Rippe, K.; Langowski, J. *Single Mol.* **2002,** *3,* 49–61.

(69) Dittrich, P.; Schwille, P. *Anal. Chem.* **2002,** *74*, 4472–4479.

(70) Winkler, T.; Kettling, U.; Koltermann, A.; Eigen, M. *Proc. Natl. Acad. Sci. USA* **1999,** *96*, 1375–1378.

(71) Heinze, K.G.; Koltermann, A.; Schwille, P. *Proc. Natl. Acad. Sci. USA* **2000,** *97,* 10377–10382.

(72) Schwille, P.; Meyer-Almes, F.J.; Rigler, R. *Biophys. J.* **1997,** *72*, 1878–1886.

(73) Petersen, N.O. *Fluorescence Correlation Spectroscopy: Theory and Applications*: Springer, Berlin, **2001**, 162–184.

(74) Heinze, K.G., Rarbach, M., Jahnz, M., Schwille, P. *Biophys. J.* **2002**, *83,* 1671-1681.

(75) Heikal, A.A., Hess, S.T., Baird, G.S., Tsien, R.Y., Webb, W.W. *Proc. Nat. Acad. Sci. USA* **2000**, *97,* 11996-12001.

(76) Schwille, P., Kummer, S., Heikal, A.A., Moerner, W.E., Webb, W.W. *Proc. Nat. Acad. Sci. USA* **2000**, *97,* 151-156.

(77) Gennerich, A., Schild, D. *Biophys. J.* **2000**, *79*, 3294-3306.

(78) Enderlein, J. *Opt. Lett.* **2000**, *25*, 634-636.

(79) Enderlein, J., Böhmer, M. *Opt. Lett.* **2003**, *28*, 941-943.

(80) Erickson, J., Goldstein, B., Holowka, D., Baird, B., *Biophys. J.* **1987**, *52*, 657-662.

(81) Moncada, S.; Palmer, R. M. J.; Higgs, E. A. *Pharmacol. Rev.* **1991**, *43*, 109-142.

(82) Li, H; Forstgermann, U. *J. Pathol.* **2000**, *190*, 244-254

(83) Moroz, L. L.; Gillette, R.; Sweedler, J. V. *J. Exp. Biol.* **1999**, *202*, 333-341

(84) Moroz, L. L. In *Nitric Oxide and Free Radicals in Peripheral Neurotransmission*, Kalsner S, ed.: New York: Springer-Verlag, 2000, pp 1-34

(85) Dinerman, J. L.; Dawson, T. M.; Schell, M. J.; Snowman, A.; Snyder, S. H. *Proc. Natl.Acad. Sci. USA* **1994**, *91*, 4214-4218

(86) Griffin, O. W.; Stuehr, D. J. *Annu. Rev. Physiol.* **1995**, *57*, 707-736

(87) Nathan, C. *FASEB J.* **1992**, *6*, 3051-3064

(88) Petit, J-F.; Nicaise, M.; Lepoivre, M.; Guissani, A.; Lemaire, G. *Biochem. Pharmacol.* **1996**, *52*, 205-212

(89) Wood, J.; Garthwaite, J. *Neuropharmac.* **1994**, *33*, 1235-1244

(90) Ding, J. M.; Chen, D.; Weber, E. T.; Faiman, L. E.; Rea, M. A.; Gillette, M. U. *Science* **1994**, *266*, 1713-1717

(91) Zafiriou, O. C.; McFarland, M; Bromund, R. H. *Science* **1980**, *207*, 637-639

(92) Kowles, R. G.; Moncada, S. *Biochem. J.* **1994**, *298*, 249-258

(93) Lopez-Figueroa, M. O.; Caamano C.; Marin, R.; Guerra, B.; Alonso, R.; Morano, M. I.; Huda, A.; Watson, S. J. *Biochim. Biophys. Acta* **2001**, *1540*, 253-264

(94) Bredt, D. S.; Snyder, S. H. *Neuron* **1992**, *8*, 3-11

(95) Saeson, T. M.; Bredt, D. S.; Fotuhi, M.; Hwang, P. M.; Snyder, S. H. *Proc. Natl. Acad. Sci. USA* **1991**, *88*, 7797-7801

(96) Hope, B. T.; Michael, G. J.; Knigge, K. M.; Vincent, S. R. *Proc. Natl. Acad. Sci. USA* **1991**, *88*, 2811-2814

(97) Zhou, X.; Arnold, M. A. *Anal Chem.* **1996**, *68*, 1748-1754

(98) Evmiridis, N. P.; Yao, D. *Anal. Chim. Acta* **2000**, *410*, 167-175

(99) Feelisch, M; Stamler, J. S. *Methods in Nitric Oxide Research*, New York: J. Wiley, 1996, pp 309-318

(100) Green, L. C.; Wagner, D. A.; Glogowski, J.; Skipper, Jr. P. L.; Wishnok, J.S.; Tannenbaum, S.R. *Anal. Biochem.* **1982**, *126*, 131

(101) Lai, C.S.; Komarov, A.M. *FEBS Letters* **1994**, *345*, 120-124

(102) Yoshimura, T.; Yokoyama, H.; Fujii, S.; Takayama, F.; Oikawa, K.; Kamada, H. *Nature Biotech.* **1996**, *14*, 992-994

(103) Ishida, Y.; Hashimoto, M.; Fukushima, S.; Masumura, S.; Sasaki, T.; Nakayama, K.; Tamura, K.; Murakami, E.; Isokawa, S.; Momose, K. *J. Pharmacol. Toxicol. Methods* **1996**, *35*, 19-24

(104) Malinski. T.; Taha, Z. *Nature* **1992**, *358*, 676-678

(105) Barker, S.L.R.; Kopelman, R.; Meyer, T.E.; Cusanovich, M.A. *Anal. Chem.* **1998**, *70*, 971-976

(106) Barker, S.L.R.; Kopelman, R. *Anal. Chem.* **1998**, *70*, 4902-4906

(107) Barker, S.L.R.; Clark, H.A.; Swallen, S.F.; Kopelman, R.; Tsang, A.W.; Swanson, J.A. *Anal.Chem.* **1999**, *71*, 1767-1772

(108) Barker, S.L.R.; Zhao, Y.; Marletta, M.A.; Kopelman, R. *Anal.Chem.* **1999**, *71*, 2071-2075

(109) Franz, K.J.; Singh, N.; Spingler, B.; Lippard, S.J. *Inorg. Chem.* **2000**, *39*, 4081-4092

(110) Nakatsubo, N.; Kojima, H.; Sakurai, K.; Kikuchi, K.; Nagoshi, H.; Hirata, Y.; Akaike, T.; Maeda, H.; Urano, Y.; Higuchi, T.; Nagano, T. *Biol. Pharm. Bull.* **1998**, *21*, 1247

(111) Kojima, H.; Nakatsubo, N.; Kikuchi, K.; Kawahara, S.; Kirino, Y.; Nagoshi, H.; Hirata, Y.; Nagano, T. *Anal. Chem.* **1998**, *70*, 2446-2453

(112) Kojima, H.; Nagano, T. *Adv. Mater.* **2000**, *12*, 763-765

(113) Itoh, Y.; Ma, F.H.; Hoshi, H.; Oka, M.; Noda, K.; Ukai, Y.; Kojima, H.; Nagano, T.; Toda, N. *Anal. Biochem.* **2000**, *287*, 203-209

(114) Katayama, Y.; Takahashi, S.; Maeda, M. *Anal. Chim. Acta* **1998**, *365*, 159-167

(115) Dybco, A. *Sensors* **2001**, *1*, 29-37

(116) Lev, O; Tsionsky, L.; Rabinovich, L.; Glezer, V.; Sampath, S.; Pankratov, I.; Gun, J. *Anal. Chem.* **1995**, *67*, 22A-30A

(117) Judeinstein, P.; Sanchez, C. *J. Mater. Chem.* **1996**, *6*, 511-527

(118) Munoz-Aguado, M.-J.; Gregorkiewitz *J. Colloid Interf. Sci.* **1997**, *185*, 459-465

(119) Ying, J. Y.; Benziger, J, B. *J. Am. Ceram. Soc.* **1993**, *76*, 2571

(120) Brinker, C. J.; Keefer, K. D.; Schaefer, D. W.; Ashley, C. S. *J. Non-Cryst. Solids* **1982**, *48*, 47

(121) Schmidt, H.; Scholze, H.; Kaiser, A. *J. Non-Cryst. Solids* **1984**, *63*, 1

(122) McDonagh, C.; MacCraith, B.D.; McEvoy, A.K. *Anal. Chem.* **1998**, *70*, 45-50

(123) Pope, E. J. A.; Mackenzie, J. D. *J. Non-Cryst. Solids* **1986**, *87*, 185

(124) Birch, D. J. S.; Geddes, C. D. *Proc. Indian Acad. Sci. (Chem. Sci.)* **2000**, *112*, 311-322

(125) Iler, R. K. *The Chemistry of Silica*, Wiley: New York, 1979

(126) Brinker, C. J.; Scherer, G. W. *Sol-Gel Science: The Physics and Chemistry of Sol-Gel Processing*, Academic Press, Inc.: New York, 1990

(127) Cornelius C. J. *Physical and Gas Permeation Properties of a Series of Novel Hybrid Inorganic-Organic Composites Based on a Synthesized Fluorinated Polyimide, Ph.D. Thesis*, Virginia Polytechnic Institute and State University, 2000

(128) Wang, P. G.; Xiang, M.; Tang, X.; Wu, X.; Wen, Z.; Cai, T.; Janczuk, A. J. *Chem. Rev.* **2002,** *102,* 1091-1134

(129) Voet, D.; Voet, J. G. *Biochemistry*, Wiley: New York, 1995

BIOGRAPHICAL SKETCH

Alina Cristina Munteanu was born in Ploiesti, Romania. Alina attended Mihai Viteazul High School in Ploiesti. She then attended University of Bucharest and studied technological biochemistry and received a Bachelor of Science degree in the spring of 1997. In fall 1998 she received a Master of Science degree in Biosensors for Environmental Analysis from University of Bucharest and University of Perpignan, France. Thereafter she further pursued a Ph.D. in bioanalytical chemistry under the supervision of Dr. Weihong Tan. She will receive her Doctor of Philosophy in analytical chemistry from the University of Florida in December of 2007.